Measurement of myofilament-localised calcium dynamics in adult cardiomyocytes and the effect of hypertrophic cardiomyopathy mutations

Alexander J Sparrow PhD[1,2], Kolja Sievert MD [1#a], Suketu Patel MSc[1,2], Yu-Fen Chang PhD[1,2,#b], Connor N Broyles Msc[1,2], Frances A Brook D.Phil[1,2], Hugh Watkins FRS MD PhD FRCP FMedSci [1,2,3], Michael A Geeves PhD[4], Charles Redwood PhD[1,2], Paul Robinson D.Phil[1,2†], Matthew J Daniels MD PhD FSCAI[1,2,3,5,6*†]

[1] Division of Cardiovascular Medicine, Radcliffe Department of Medicine, University of Oxford, Oxford, UK

[2] BHF Centre of Research Excellence, University of Oxford, Oxford, UK

[3] Department of Cardiology, Oxford University NHS Hospitals Trust, Oxford, UK

[4] Department of Biosciences, University of Kent, Canterbury, UK

[5] BHF Centre of Regenerative Medicine, University of Oxford, Oxford, UK

[6] Department of Biotechnology, Graduate School of Engineering, Osaka University, Suita, Osaka, Japan

[#a]Current address: CardioVascular Center Frankfurt (CVC), Seckbacher Landstr. 65, 60389, Frankfurt, Germany

[#b]Current address: Lumistar Biotechnology Inc., Zebulon Business Center 2F, No.467, Sec. 6, Zhongxiao E. Rd., Nangang Dist., Taipei City 115, Taiwan

* Correspondence to: Dr Matthew J Daniels, Division of Cardiovascular Medicine, Radcliffe Department of Medicine, University of Oxford, Level 6, West Wing, John Radcliffe Hospital, Headley Way, Headington, Oxford, OX3 9DU, UK. Email: matthew.daniels@cardiov.ox.ac.uk

† These authors contributed to the work equally

Short Title: Myofilament-localised calcium dynamics in HCM

Total word count: 7985

Subject codes: Calcium Cycling/Excitation-Contraction Coupling, Mechanisms, Cardiomyopathy, Hypertrophy

Abstract

Rationale: Subcellular Ca^{2+} indicators have yet to be developed for the myofilament where disease mutation, or small molecules may alter contractility through myofilament Ca^{2+} sensitivity. Here we develop and characterise genetically encoded Ca^{2+} indicators restricted to the myofilament to directly visualise Ca^{2} changes in the sarcomere.

Objective: To produce and validate myofilament restricted Ca^{2+} imaging probes in an adenoviral transduction adult cardiomyocyte model using drugs that alter myofilament function (MYK-461, omecamtiv mecarbil and levosimendan) or following co-transduction of two established hypertrophic cardiomyopathy (HCM) disease causing mutants (cTnT R92Q and cTnI R145G) that alter myofilament Ca^{2+} handling.

Methods and Results: When expressed in adult ventricular cardiomyocytes RGECO-TnT/TnI sensors localise correctly to the sarcomere without contractile impairment. Both sensors report cyclical changes in fluorescence in paced cardiomyocytes with reduced Ca^{2+} on and increased Ca^{2+} off rates compared with unconjugated RGECO. RGECO-TnT/TnI revealed changes to localised Ca^{2+} handling conferred by MYK-461 and levosimendan, including an increase in Ca^{2+} binding rates with both levosimendan and MYK-461 not detected by an unrestricted protein sensor. Co-adenoviral transduction of RGECO-TnT/TnI with HCM causing thin filament mutants showed that the mutations increase myofilament [Ca^{2+}] in systole, lengthen time to peak systolic [Ca^{2+}], and delay [Ca^{2+}] release. This contrasts with the effect of the same mutations on cytoplasmic Ca^{2+}, when measured using unrestricted RGECO where changes to peak systolic Ca^{2+} are inconsistent between the two mutations. These data contrast with previous findings using chemical dyes that show no alteration of [Ca^{2+}] transient amplitude or time to peak Ca^{2+}.

Conclusions: RGECO-TnT/TnI are functionally equivalent. They visualise Ca^{2+} within the myofilament and reveal unrecognised aspects of small molecule and disease associated mutations in living cells.

Key Words: Hypertrophic cardiomyopathy, Calcium, Contractility, Genetically encoded Ca^{2+} indicators

Non-standard Abbreviations and Acronyms:

CaM	Calmodulin
CaMKII	Ca^{2+}/calmodulin dependant kinase II
cAMP	Cyclic AMP
GECI	Genetically encoded calcium indicator
GFP	Green fluorescent protein
GPCM	Guinea pig cardiomyocyte
HCM	Hypertrophic cardiomyopathy
MOI	Multiplicity of infection
NCX	Sodium calcium exchanger
PLN	Phospholamban
TnC	Troponin C
TnI	Troponin I
TnT	Troponin T
RyR	Ryanodine Receptor
SERCA	Sarco-endoplasmic reticulum ATPase
SR	Sarcoplasmic reticulum
T_{50}	Time to 50%
WT	Wild Type

Introduction

The myofilament converts the chemical energy of ATP into mechanical energy, a process regulated by Ca^{2+}. Mutations in myofilament components cause common (1:500) inherited conditions like hypertrophic cardiomyopathy (HCM)[1,2,3]. HCM causing mutations produce hypercontractility, energetic compromise[4-6] and change Ca^{2+} utilization within the cardiomyocyte. Altered intracellular Ca^{2+} may be directly proarrhythmic, causing sudden death, and activate hypertrophic signalling pathways that produce the cardiac hypertrophy, and premature heart failure, observed in HCM patients. Interestingly, increased myofilament Ca^{2+} affinity arises from different mutations[7,8]. Prevalent thick filament mutations increase the Ca^{2+} sensitivity of contractility by altering acto-myosin affinity and modifying conformational changes in the myosin motor domain[9]. Conversely, thin filament mutations in the regulatory components troponin T (TnT) and I (TnI) increase the affinity of troponin C (TnC) for Ca^{2+}. Some consequences of trapping Ca^{2+} in the sarcomere by the introduction of Ca^{2+} sensitizing HCM mutations are known[10-12]. Briefly, raised myofilament Ca^{2+} binding produces secondary alterations in cytoplasmic and SR [Ca^{2+}] in addition to altered activation/regulation of key Ca^{2+} handling proteins (e.g. Ryanodine Receptor, SERCA2a and phospholamban). Hypertrophic signalling via calcineurin/NFAT and ERK promotes cellular hypertrophy[13]. These factors, combined with altered mechanosensing[14] and energetics[2,15], drive the stereotyped end-organ changes seen in patients.

Ca^{2+} cycling changes in HCM are typically assessed using chemical Ca^{2+} dyes[10,11,13]. However, dyes are not spatially restricted [16-19] and thus report whole cell phenomena. The patch clamp technique[20] can resolve subcellular Ca^{2+} events[10,11] but is technically challenging and low throughput. Genetically encoded calcium indicators (GECIs) offer an alternative strategy for Ca^{2+} assessment[17,19], and may be restricted to subcellular compartments by a defined sequence tag or protein fusion. Myofilament specific calcium probes remain elusive, in part due to the concern that the bulky 30x40x70Å adducts of the smallest GECIs[21] are unlikely to be tolerated by the paracrystalline sarcomeric environment[22,23] leading to perturbed function of the indicator, the fusion partner, or the cell. However, fluorescence resonance energy transfer-based cAMP indicators conjugated to myofilament proteins that do not affect cardiomyocyte contractility have been reported[24].

GECIs are available with different calcium sensor domains, tuned to different affinities, in a range of spectral hues. The CaM/M13 calcium sensor domain appears in most of the indicators successfully reported in cardiomyocytes, but not all GECIs work in all cardiac models[17]. For example, tools improved for neuronal applications may lose functionality in cardiac cells[17] eg TN-XL[25] and TN-XXL[26]. Subcellular targeting of GECIs within cardiomyocytes to probe Ca^{2+} in the SR[27] and, by conjugation of GCaMP2.2 to FKBP12.6, Ca^{2+} efflux from the SR[28] has been demonstrated. These probes visualise the Ca^{2+} store, but currently no equivalent tool to study Ca^{2+} at the myofilament, where Ca^{2+} regulates contraction exists.

Since contractility underpins cardiac function there is interest in development of small molecule modulators of myofilament contractility[22,29-31]. Importantly these agents should not affect Ca^{2+} handling, which may be pro-arrhythmic. Application of unrestricted, or myofilament localised, indicators may give greater mechanistic insight into this subclass of drugs, which include the myosin ATPase inhibitor MYK-461[30], a novel therapy for hypertrophic cardiomyopathy, and levosimendan[31] a myofilament activator developed for heart failure.

Here we produce, and characterize myofilament localized Ca^{2+} sensors to directly visualize changes in Ca^{2+} flux at the myofilament occurring in response to small molecules or disease causing mutations. We reveal how two well characterised thin filament HCM causing mutations in cTnT (R92Q)[4,10,32,33] and cTnI (R145G)[10,34-36] are from a Ca^{2+} handling perspective mechanistically similar at the myofilament, but distinct in the cytoplasm. The combination of probes reveals biology previously inferred. The method increase scale, reduces animal use, and is compatible with existing imaging infrastructure and single cell protocols.

Materials and Methods

Isolation of guinea pig left ventricular cardiomyocytes

This investigation was approved by the Animal Welfare and Ethical Review Board at the University of Oxford and conforms to the UK Animals (Scientific Procedures) Act, 1986, incorporating Directive 2010/63/EU of the European Parliament. As described[10], left ventricular cardiomyocytes were isolated from male (to prevent confounding effects of hormonal cycle) adolescent (400 g) guinea pig hearts by collagenase perfusion for 5 minutes then placed on a shaker for a further 10 minutes. Left ventricular cardiomyocytes ($1.5x10^5$ cells per ml) were incubated in $ACCITT_3$ culture medium[37] at 37°C and 5%CO_2.

Adenoviral Transduction

RGECO-TnT (plus BamHI linker) and RGECO-TnI (plus XhoI linker) were cloned into a shuttle vector. RGECO and RGECO-TnI adenoviruses were generated, purified and titred by Welgen, Inc. (Worcester, MA, USA). RGECO-TnT, WT cTnT, cTnT R92Q, WT cTnI, and cTnI R145G adenoviruses were generated as described[10]. Immediately after isolation GPCMs were adenovirally co-transduced for 48 hours with RGECO (MOI=444) and either WT cTnT (795), cTnT R92Q (933), WT cTnI (795), or cTnI R145G (795). Co-transductions of RGECO-TnT (MOI=795) were with either WT cTnI (795), or cTnI R145G (1590). Co-transductions of RGECO-TnI (MOI=444) were with either WT cTnT (795) or cTnT R92Q (1493).

Protein purification

N- and C-terminal eGFP conjugates of human recombinant TnT, TnI and TnC were cloned into pMW172 vector using 3' NdeI and 5' EcoRI restriction sites and an internal HindIII restriction site linker. RGECO and RGECO-TnT were similarly sub-cloned into pMW172. Proteins were expressed in BL21-DE3(pLysS) E.coli induced using 0.4mmol/L Isopropyl β-D-1-thiogalactopyranoside for 4 hours. Bacterial pellets recovered by centrifugation (10,000xg for 10mins) were lysed in buffer containing 25mmol/L Tris-HCl, pH 7.5, 20% sucrose, 1mmol/L EDTA, 200mmol/L NaCl,5 mol/L urea, 0.1% Triton X-100. All proteins were purified using an AKTA-UPC900 FPLC using HiTrap FF chromatography columns (GE Healthcare, Amersham). GFP-TnT and TnT-GFP were purified using sequential cation (in buffer containing 6mol/L urea, 1mmol/L EDTA, 1mmol/L 2-mercaptoethanol, 20mmol/L MOPS, pH 6.0) followed by anion (in buffer containing 6mol/L urea, 1mmol/L EDTA, 1mmol/L 2-mercaptoethanol 50mmol/L Tris-HCl pH 8.0) exchange chromatography. GFP-TnC and TnC-GFP were purified by anion (pH 8.5) exchange chromatography. GFP-TnI and TnI-GFP were purified by sequential cation and anion exchange chromatography. RGECO and RGECO-TnT were purified using sequential anion (pH 8.0) exchange chromatography, ammonium sulphate fractionation (to 50% for RGECO and 35% for RGECO-TnT) and finally Hydrophobic Interaction Chromatography (HIC) (in buffer containing 30% ammonium sulphate, 200mmol/L $NaCl_2$ 1mmol/L ditiothretol and 30mmol/L 4-(2-hydroxyethyl)-1-piperazineethanesulphonic acid (HEPES)). Ion exchange columns were eluted using a 0-2mol/L NaCl gradient, the HIC column was eluted with a 30–0% ammonium sulphate gradient. 6-Histidine-tagged RGECO-TnI was cloned into a PET23a vector and expressed as above, and purified using a HisTrap HP column (GE Healthcare) in a buffer containing 15.48mmol/L Na_2HPO_4, 4.52mmol/L NaH_2PO_4, 500mmol/L NaCl, and 6mol/L Urea (Histag buffer), followed by washing in Histag buffer with 20mmol/L Imidazole (pH 7.0), then eluted in an increasing Histag buffer gradient containing 500mmol/L Imidazole (pH 7.0). Eluted fractions were assessed for purity using 12% SDS-PAGE gels, stained with Coomassie brilliant blue. Histag was cleaved using a thrombin kit (Merck) following the manufactures instructions. Wild type human recombinant TnT, TnI, TnC and Ala-Ser-α-TM[39] were purified as previously described[38]. Troponin complex containing either WT, GFP-TnT, TnT-GFP, GFP-TnC, TnC-GFP, GFP-TnI, or TnI-GFP were reconstituted by dialysis into buffer containing 10mmol/L imidazole pH 7.0, 1mmol/L DTT, 0.01% azide, 0.1mol/L $CaCl_2$, 6mol/L urea and 1mol/L KCl. Urea was reduced stepwise from to 2 then 0mol/L, then KCl was reduced stepwise from 1mol/L to 800 – 600 – 400 – 200mmol/L KCl in a series of 3 hour dialyses. Tn Complex was purified using size exclusion chromatography in 200mmol/L KCl dialysis buffer. Purity was analysed by SDS-

PAGE. Purified troponin complexes were dialysed into buffer containing 5mmol/L 1,4-Piperazinediethanesulphate pH 7.0, 3.87mmol/L $MgCl_2$, 1mmol/L DTT for ATPase assay experiments. Actin and myosin-S1 was extracted from rabbit skeletal muscle as described[39, 40].

In vitro acto-myosin ATPase assays

ATPase assays were carried out as described[8, 38]. Briefly, a master stock of 3.5µmol/L actin, 0.5µmol/L myosin S1, 0.5µmol/L Ala-Ser-α-TM and 0.5µmol/L Tn complex were mixed in buffer containing 5mmol/L 1,4-Piperazinediethanesulphate pH 7.0, 3.87mmol/L $MgCl_2$, and 1mmol/L DTT. To ensure precise thin filament protein stoichiometry, each stock was centrifuged at 384000xg for 15 minutes. Recovered pellets were aliquoted and set to a range of $[Ca^{2+}]_{free}$ from pCa 4.5-8.5 using Maxchelatior (http://maxchelator.stanford.edu/CaEGTA-TS.htm). ATPase reactions were initiated by addition of 3mmol/L ATP and incubated at 37°C for 15 minutes. Each reaction was quenched in 5% TCA, finally 1% ammonium molybdate in 0.5mol/L H_2SO_4, followed by 40% iron(II)sulphate in 0.5mol/L H_2SO_4 was used to measure inorganic phosphate. Absorbance (A_{700}) measurements were converted to absolute activity (sec^{-1}). Calcium-sensitivity data was fitted to the Hill equation using KaleidaGraph (Synergy Software).

Hill equation: $$A = \frac{A_{min}+(A_{max}-A_{min})}{1+10^{((pCa-pCa_{50})\times n_H)}}$$

Where: A=ATPase rate; A_{min}=Minimum ATPase rate; A_{max}=Maximum ATPase rate; pCa=-log $[Ca^{2+}]$; pCa_{50}=- log $[Ca^{2+}]$ required for half maximum ATPase activity; n_H=Hill coefficient.

Calcium binding K_d calculations

For steady state Ca^{2+} binding affinity (K_d) for RGECO, RGECO-TnI and RGECO-TnT, 3µmol/L of protein was dialysed into buffer containing 130mmol/L NaCl, 10mmol/L 4-(2-hydroxyethyl)-1- piperazineethanesulphonic acid (HEPES), 1mmol/L dithiothretol, 1.3mmol/L $MgCl_2$, pH 7.3. A range of $_{free}[Ca^{2+}]$ conditions were set between 3.16nmol/L (pCa 8.5) and 31.6µmol/L (pCa 4.5) using 1mmol/L EGTA and the corresponding concentration of $CaCl_2$. Steady state fluorescence readings were made in an Ultraclear bottom 96-well microplate using a FLUOstar Omega plate reader (BMG LABTEC, Germany), using 544nm excitation and 590/10nm emission filters at both 25 and 37°C. Fluorescence emission intensities were plotted vs $_{free}[Ca^{2+}]$ and fitted to the Hill equation to calculate K_d values for each protein and condition. For Ca^{2+} displacement (k_{off}), 125nmol/L RGECO-TnT plus 5µmol/L $CaCl_2$ was mixed with 5mmol/L EGTA in a buffer containing 130mmol/L NaCl, 10mmol/L 4-(2- hydroxyethyl)-1-piperazineethanesulphonic acid (HEPES) 1.3mmol/L $MgCl_2$, 1mmol/L dithiothretol, pH 7.3 with NaOH. RGECO or RGECO-TnT was loaded into a Stopped-flow system (HiTech Scientific, Bradford-on-Avon, UK), concentrations after mixing 1:1 in the stopped-flow. Fluorescence was excited at 546nm (100W Xe/Hg lamp and monochromator) and emission monitored through an OG-590 glass filter. Data was fitted to a single exponential decrease in fluorescence of 50-100%, depending upon temperature. For calcium binding (k_{on}), 125nmol/L RGECO-TnT was measured at 10µmol/L free calcium by mixing with a buffer containing 2.125mmol/L Ca. EGTA and 0.2mmol/L EGTA with the same filter set as before. Fluorescence increase upon Ca^{2+} addition was fitted to a single exponential. The observed single exponential rate constant, k_{obs}, was extracted for k_{on} and k_{off} for both sensors, at a range of temperatures between 25 and 37°C. To estimate the dissociation constant, we using the equations $K_d = k_{obs}$-off [Ca]/ k_{obs} on; these were comparable to steady state K_d values.

Determination of Quantum Yield and Molar Extinction Co-efficient

Quantum yield and molar extinction co-efficient was determined for each Ca^{2+} sensor following[41]. Quantum yield standards were mCherry (for RGECO) and RGECO for RGECO-TnT. The concentration of protein in buffer containing 10 mM HEPES, 1.3mmol/L $MgCl_2$ and 1mmol/L dithiothreitol was determined using BCA assay (Pierce) and set to either pCa 4.5 of 8.5.The protein concentration was reduced to an absorbance at the excitation wavelength between 0.2 and 0.6. Dilutions to absorbance's of 0.01, 0.02, 0.03 and 0.04 were made for each protein solution and standard. The fluorescence emission spectra at Ex F_{568} were recorded using an RF-1501

spectrofluorimeter (Shimadzu, Japan). Total fluorescence intensities were obtained by integration. Integrated fluorescence intensity vs. absorbance was plotted for each protein and each standard. Quantum yields were determined from the slopes (S) of each line using the equation: Φprotein = Φstandard × (Sprotein/Sstandard). Extinction coefficients were determined from the absorption spectrum of both RGECO and RGECO-TnT at pCa 8.5 and 4.5 in the buffer above using a plate reader (BMG LABTECH, Germany). Peak Absorbance wavelengths were determined to be A_{465} in low Ca^{2+} and A_{581} in high Ca^{2+}. Absorbance measurements were converted to 1 cm path length using BMG Omega software. Extinction coefficients were calculated by dividing the peak absorbance maximum by protein concentration.

Immunofluorescence

GPCMs were fixed in 4% paraformaldehyde, washed in PBS, permeabilized and blocked in 0.1% Triton X-100, 3% BSA in PBS. Primary antibodies (1:500 anti-alpha actinin (Sigma, clone EA-53, A7811), 1:200 anti-DsRed (Clontech, 632496), 1:8 anti-Flagtag (Sigma, F1804)) were added overnight at 4°C, washed in PBS, and secondary antibodies added (goat anti-rabbit IgG Alexa 568 (1:200) (Invitrogen, A21069) and goat anti-mouse IgG Alexa 633 (1:200) (Invitrogen, A21053)) for 1 hour at room temperature, washed in PBS and mounted on slides in ProLong Diamond antifade with DAPI (ThermoFisher). Slides were imaged on a Leica TCS SP5 confocal microscope with a 63x oil immersion lens, images data was extracted with Leica LAS and ImageJ (NIH, USA). Control slides were prepared excluding the primary antibody for all IF experiments, negligible background fluorescence was detected in all cases.

Subcellular fractionation and western blotting

GPCMs were fractionated to recover cytoplasmic and sarcomeric/cytoskeletal samples following[42]. 300,000 cardiomyocytes were centrifuged, re-suspended in buffer containing, 20mmol/L Tris-HCl pH 7.4, 2mmol/L EDTA, 0.5mmol/L EGTA, 0.3mmol/L sucrose and homogenised for 1 minute. Cells were pelleted at 1000xg for 5mins, the supernatant/cytoplasmic fraction was retained for SDS-PAGE analysis and western blotting. The cell pellet was washed 3 times in fractionation buffer + 1% Triton X-100 each time pelleting the sarcomeric fraction by centrifugation at 1000xg for 5mins. Finally, the sarcomeric fraction was re-suspended in fractionation buffer (without Triton X-100) and prepared for western blotting. Subcellular fractions and GPCM lysates were run on a 12% polyacrylamide gel, transferred onto PVDF membrane, and blocked with 5% bovine milk in Tris buffered saline, 0.1% Tween-20 (TBS-T) for 1hour. Primary antibodies were incubated overnight at 4°C in 5% bovine milk in TBS-T (1:2000 anti-cTnT (Sigma, SAB2108239), 1:4000 anti-ERK (Cell Signaling Technologies, 4695s), 1:5000 anti-FLAG-tag (Sigma, F3165), 1:10000 anti-GAPDH (Millipore, ABS16), 1:2000 anti-TnI (TNNI3, Aviva Systems Biology, ARP41391_P050). Membranes washed in TBS-T were incubated in secondary antibodies (1:10000 anti-rabbit HRP (GE Healthcare, NA934), 1:10000 anti-mouse HRP (GE Healthcare, NA931)) for 1 hour at room temperature, washed in TBS-T then developed with ECL select (GE Healthcare) and imaged on a ChemiDoc MP (BioRad). Densitometric measurements to compare single verses double infected levels of FLAG-tag protein were carried out using Image Lab software (BioRad), and normalised to GAPDH loading controls for each comparison.

Sarcomere length measurements

Sarcomere length measurements were performed using IonOptix μstep apparatus and the manufacturers' standard operating instructions. Cells, electrically paced at 40 volts, 0.5 Hz, 37°C were perfused with buffer containing 150mmol/L NaCl, 10mmol/L HEPES, 7mmol/L glucose, 1mmol/L $MgCl_2$, 1mmol/L KCl, 0.3mmol/L NaH_2PO_3, 1.8mmol/L $CaCl_2$, at pH 7.4. Cells displaying asynchronous contractility, excessive blebbing/dysmorphology were ignored for acquisition. Similarly cells with contractile magnitudes or velocities exceeding 2 standard deviations from the mean upon analysis were also excluded due to phenotypic heterogeneity arising in cultured primary cells.

Imaging and analysis

GPCMs imaged on an Olympus IX81 inverted microscope (Olympus, Japan) with a C-1900 EMCCD camera (Hamamatsu, Japan) were electrically paced at 0.5Hz in a humidified chamber at 37°C. Videos (28seconds, 25fps) were acquired through an Olympus UPlanFLN 10x lens (NA 0.3) with the RFP filter set of 560/25 nm (excitation), 620/60 nm (emission) with a 565 nm dichroic mirror using CellR software (Olympus) as previously described[43]. RGECO, RGECO-TnI and RGECO-TnT adenovirally transduced GPCMs were incubated with 250nmol/L MYK-461, 200µmol/L omecamtiv mecarbil or 10µmol/L levosimendan 20mins before imaging. For Fluo-4 comparison, RGECO-TnT transduced cardiomyocytes were loaded with 1µmol/L Fluo-4 as per the manufacturer's instructions for 5minutes and imaged using RFP and GFP (485/20-25 nm (excitation), 525/50 nm (emission) with a 495 nm dichroic mirror) filter sets.

Raw image data was extracted using CellR (Olympus), and analysed in Excel (Microsoft). From a single cell, 10 transients were extracted and averaged to give a single transient in a 2 second interval per cell. Time to 50% contraction, time to 50% baseline (from peak), time of peak, or time above 50% was determined. Peak intensity analysis was performed as previously described for intensiometric sensors[44, 45]

$$\frac{\Delta F}{F} = \frac{F(t) - F(min)}{F(min)} \times 100$$

Where F(t) is the fluorescence intensity at time (t), and F(min) the minimum fluorescence intensity during the averaged transient.

Statistics

For all single cells experiments, comparisons were from at least three separate cell isolations, where approximately equal numbers of cells (±5) were taken from each preparation on an experiment-to-experiment basis. Data was firstly tested for normality (D'Agostino-Pearson). Sarcomere length measurements were made using unpaired Students t-test. Wilcoxon T-test was used for the comparison of Fluo-4 to RGECO-TnT. RGECO to RGECO-TnT/TnI and pacing frequencies were compared using non-parametric Kruskal-Wallis one-way ANOVA. Drugs and WT to mutant troponin were compared using non-parametric Mann-Whitney test (Graphpad Prism). Once acquired, all data was blinded prior to extraction and analysis.

Results

Development and In vitro characterisation of myofilament RGECO Ca^{2+} sensors

To develop a myofilament-restricted GECI, fusion proteins of green fluorescent protein (GFP) at the N- and C-terminus of each troponin subunit were screened to identify sites preserving in vitro acto-myosin ATPase Ca^{2+} dependent regulation. GFP conjugation to the N-terminus of either TnT or TnI maintained Ca^{2+} regulation (Figure 1, Online Table I). Subsequently, the red GECI RGECO[41] was conjugated to the N-terminus of troponin-T and troponin-I (Online Figure X, XI). In vitro characterisation of the calcium indicator properties of RGECO-TnT and RGECO-TnI showed K_d of 764.5±17.6nmol/L, and 657.3±27.3nmol/L respectively under physiological pH[46], temperature and magnesium concentration[47] (Online Figure I), with preservation of dynamic range and excitation/emission spectra (Figure 2A-C, Online Table II). This is compatible with previous reports[41] (RGECO K_d = 484nmol/L at 25°C and 3mmol/L $MgCl_2$). At physiological temperature, Ca^{2+} on (k_{obs} 16.7µmol/L^{-1}s^{-1} at 10µmol/L free Ca^{2+}) and off (k_{off} = 16.9s^{-1}) rates for myofilament RGECO were approximately twice those observed at 25ºC (Online Figure II). Importantly in intact, but unloaded, GPCMs the presence of RGECO-TnT/TnI did not affect sarcomere shortening compared to uninfected controls (Figure 2D and E, Online Figure III).

Characterisation of RGECO-TnT and RGECO-TnI Ca^{2+} sensors in cardiomyocytes

RGECO-TnT or RGECO-TnI localize to the sarcomere, without Z-disk accumulation, following adenoviral transduction of GPCMs. Conversely, unconjugated RGECO is broadly distributed with weak Z-disk accumulation (Figure 3A, Online Figure IV). 48 hours following viral infection, total TnI contained 58.7±11.0% (n=5) RGECO-TnI and similarly TnT contained 54.3±5.5% (n=4) RGECO-TnT (Figure 3B and C). RGECO-TnI and RGECO-TnT both show cyclical fluorescence in paced cardiomyocytes (Figure 3D and E), with equivalent kinetics in untreated GPCMs stimulated at 0.5Hz (Figure 3F, Online table III). The on and off rates of fluorescence differ in both myofilament localised indicators compared to the unrestricted RGECO. On rates were significantly slower (ΔT_{50} on = 47±5 and 39±4msec for RGECO-TnT and RGECO-TnI respectively), whilst off rates were significantly faster (ΔT_{50} off = -26±8 and -41±11msec for RGECO-TnT and RGECO-TnI respectively) than unrestricted RGECO (Online Table III). Interestingly, these rate differences are qualitatively preserved when RGECO-TnT emissions are compared to the chemical dye Fluo-4 (Online Figure V).

To explore the sensitivity of RGECO-TnI/RGECO-TnT to detect changes in Ca^{2+} transient duration or magnitude that might be provoked by small molecules or disease causing mutations we performed a series of experiments with well annotated modifiers of cardiac physiology. To ensure changes in Ca^{2+} kinetics can be observed we used the reverse-rate dependence phenomenon that accompanies increasing frequency of electrical stimulation. All genetically encoded probes respond to increased pacing frequencies (0.5, 1 and 2 Hz) with increased speed of binding and release as the Ca^{2+} transient duration shortens (Online Figure VI). Since the lowest pacing frequency produces the longest Ca^{2+} transient, and maximizes experimental duration, we performed subsequent experiments at 0.5 Hz.

Small molecule effects on cytoplasmic and myofilament Ca^{2+} dynamics

To investigate the ability of RGECO-TnI/RGECO-TnT to detect localized changes in Ca^{2+} compared to an unrestricted sensor we used three small molecule modulators of myofilament contractility. MYK-461 was selected as a myosin ATPase inhibitor (Figure 4). Omecamtiv mecarbil, which increases the interaction between actin and myosin independently of Ca^{2+} was selected as a myosin activator (Figure 5), and finally, the inodilator levosimendan which stabilizes the Ca^{2+} bound form of TnC activating the myofilament (Figure 6). In agreement with previous observations[48] omecamtiv mecarbil did not change any aspect of the Ca^{2+} transient with any probe (Figure 5). By contrast, peak amplitudes increase in the presence of levosimendan, and reduce in the presence of MYK-461. The myofilament restricted indicators report greater changes in peak amplitude ratio compared to the unrestricted control. The relative reductions in fluorescence conferred by MYK-461 were -9.5±3.8 %, -21.4±4.3% and -42.7±4.1% for RGECO, RGECO-TnT and RGECO-TnI respectively. Analogous increases in fluorescent amplitude following levosimendan treatment were +47.5±6.6%, +198.8±23.8% and +170.8±16.5% for RGECO, RGECO-TnT and RGECO-TnI respectively. Additionally, the myofilament localised RGECO reveals changes to the rate of Ca^{2+} binding and release in the presence of both MYK-461 and levosimendan contrasting with the results obtained with the cytoplasmic probe (Figure 4 and 6). Both myofilament restricted indicators in response to 250 nM MYK-461 and 10 μM levosimendan reduce the T_{50}On times (RGECO-TnT -0.031±0.002 sec, -0.008±0.002 sec; RGECO-TnI -0.019±0.004 sec to -0.018±0.002 sec for MYK-461 and levosimendan respectively) whilst RGECO detects no change. Interestingly the unrestricted RGECO reports greater changes to T_{50}Off compared to the restricted sensors (Figure 4, and 6), which might reflect hierarchical Ca^{2+} reuptake. Importantly, neither compound affects the intrinsic Ca^{2+} sensor function of RGECO-TnT (Online Figure VII).

Cytoplasmic and myofilament localised Ca^{2+} dynamics in HCM

Small molecule action in intact cells may include both on- and off-target components. Therefore, we explored whether the targeted RGECO strategy identified alterations in the calcium transient driven by HCM causing mutations, which should principally work through the myofilament. Specifically, previous contractility data suggests that peak amplitude should increase, and also phase shift by ~100 msec, however these have been undetectable with fura-2[8]. Recombinant adenovirus expressing RGECO-TnT was used to study the effects of wild type (WT) cTnI or cTnI R145G

expression; conversely, adenovirus expressing RGECO-TnI was used to observe the effects of WT cTnT or cTnT R92Q in GPCMs. The mutually exclusive expression of HCM mutant protein and sensor conjugate allows changes in Ca^{2+} flux to be attributed to the mutation independently of the consequence of the mutation itself.

Previously we showed a mutant transgene expression approach models autosomal dominant human HCM (~54% for cTnT R92Q and ~49% for cTnI R145[10]) and produces hypercontractility as a cellular manifestation of disease phenotype. Here, as we co-transduced separate adenoviruses containing the disease gene and the complementary Ca^{2+} indicator, adjustments to expression levels of singly verses doubly transduced cells required optimization of the multiplicities of infection (MOI), with subsequent western blot analysis to ensure doubly transduced cells had equivalent FLAG-tagged protein expression to singly transduced cells[10] (Online Figure VIII). Immunolocalization experiments using DsRed and FLAG-tag antibodies to detect RGECO and HCM mutant troponin show no alterations to protein localization or sarcomeric structure as previously described[10] (Online Figure IX)

At the myofilament, compared to the WT control, both cTnT R92Q and cTnI R145G exert similar effects. The peak amplitude is delayed and elevated combined with slower T_{50} release times indicative of HCM causing thin filament mutations promoting more Ca^{2+} at the myofilament for longer intervals. Conversely, the whole cell indicator reports differential changes in peak systolic Ca^{2+} only for cTnI R145G, and no change in systolic Ca^{2+} for cTnT R92Q (Figure 7A-E, Online Table IV). The delay in time of peak Ca^{2+} correlates with previously published sarcomere length traces showing a delayed peak contraction time, which are overlooked by chemical dyes[10]. All indicator combinations detected increased time to 50% binding in both cTnT R92Q and cTnI R145G (Figure 7F, Online Table IV) and T_{50} release predicted (Online Table IV) from previous work measuring whole cell Ca^{2+} dynamics[10].

Discussion

Here we show that a genetically encoded Ca^{2+} sensor, RGECO, can be targeted to the myofilament without perturbing contractility, or indicator function. This allows direct Ca^{2+} measurement in a key compartment of the cardiomyocyte historically studied indirectly. The availability of two targeted sensors, which are almost functionally equivalent, should facilitate studies of calcium handling at the myofilament in response to drugs or disease causing mutation.

GECIs applied to GPCMs reveal findings that contrast with calcium dyes. For example GECIs show the myosin ATPase inhibitor MYK-461 alters Ca^{2+} binding, release and signal amplitude, none of which were previously described in chemical dye studies[30]. Furthermore, myofilament targeting enhances the observed effect size when cardiomyocytes are treated with levosimendan. The mechanism of levosimendan action is debated, with a direct Ca^{2+} sensitizing effect meditated through TnC, a cAMP mediated effect through phosphodiesterase III inhibition[49], and mitochondrial potassium channel activation[50] all reported. While our data do not define the relative contributions, or the intermediates in the mode of action, they do show potent elevation of myofilament Ca^{2+} is combined with an increase in total cell Ca^{2+}. The whole cell consequences are undesirable, and possibly attributable to off-target effects, as the R92Q-TnT mutant demonstrates that increased myofilament Ca^{2+} need not translate into increased whole cell Ca^{2+}. Similarly, omecamtiv mecarbil[48] alters contraction but does not change Ca^{2+} at the whole cell, or myofilament level in this model.

The myofilament restricted Ca^{2+} indicators reveal both cTnT R92Q and cTnI R145G HCM causing variants increase myofilament peak Ca^{2+} and delay release. Therefore the increased myofilament Ca^{2+} affinity common to both mutations[8] directly correlates with increased microdomain $[Ca^{2+}]$. This is compatible with previous work showing the same mutations increased myofilament Ca^{2+} buffering and altered $[Ca^{2+}]$ inferred by a rise in diastolic fura2 fluorescence[10]. The RGECO-TnI/TnT data contrast with results from the unrestricted RGECO indicator; where systolic peak intensity differences are observed only for cTnI R145G (a large increase) but not cTnT R92Q

suggesting distinct consequences of these mutations. Since prior work excluded other factors such as fractional Ca^{2+} release from the SR[10], the differences appear determined by what happens at the myofilament. This is mechanistically plausible as the cTnI R145G mutation directly increases Ca^{2+} binding to the regulatory site (I) of cTnC, whereas cTnT R92Q is structurally distant from the Ca^{2+} binding sites in the troponin complex and sensitizes myofilament Ca^{2+} binding via alterations to co-operative communication[8]. Furthermore previous studies show the cTnI R145G mutation has a greater effect on Ca^{2+} buffering than TnT R92Q (TnT R92Q ΔK_d=582nmol/L, TnI R145G ΔK_d=1082nmol/L compared to WT)[10]. We believe greater severity of the R145G mutation, which has a more pronounced contractility effect[8], underpins the differential observations of changes to bulk Ca^{2+} with RGECO between the two mutants although exactly what makes the R145G cTnI mutation more severe is unknown. Interestingly a CRISPR engineered thick filament HCM iPS-CM model (MYH7 R453C) has raised peak systolic Ca^{2+} visualized by unrestricted RGECO[51]. From this we postulate that cytoplasmic Ca^{2+} increases could be a hallmark of some HCM causing mutations. This raises an important, potentially clinically significant, concept. HCM represents a common clinical end-point of many different mutations. There is an unmet need to understand the shared and distinct consequences of individual mutations. Common mechanisms central to disease pathogenesis may be preferable as therapeutic targets, but they may leave residual aspects of individual mutations untreated. The impact of this is currently uncertain, but we may gain insight in to this through trials such as EXPLORER investigating MYK-461 in HCM cohorts.

Ca^{2+} overload specifically at the myofilament is thought to activate hypertrophic signalling pathways as a component of the HCM disease mechanism[13, 52, 53], however measuring this directly in living cells has remained elusive. This is the first study to not only show this occurs, but also that the phase shift in contractility is paralleled by a shift in the Ca^{2+} transient using any of the three protein indicators tested. These indicators simplify, and accelerate the process of studying Ca^{2+} dynamics at the myofilament without the need for multiple inferred observations of total and free Ca^{2+} using simultaneous patch clamping and chemical Ca^{2+} dyes[10, 11, 20]. Although the proteins used to detect Ca^{2+} are physically bulky and may have unmeasured effects on the intricate structure of the myofilament, or myofilament Ca^{2+} buffering capacity, contractile impairment is not seen in the GPCM transient expression model; this contrasts with the chemical dyes typically used to study Ca^{2+}[10, 54]. A limitation of the RGECO indicators is their intensiometric nature, which precludes robust calibration allowing an observed signal to be converted to $[Ca^{2+}]$. However, GECIs reveal changes in Ca^{2+} amplitude and kinetics that are overlooked with dye based probes. This opens a new investigative pathway in understanding this important microdomain within contractile cells which should be generally applicable to conditions affecting cardiac contractility and Ca^{2+} handling. They improve the fidelity of screening tools for small molecule evaluation in the heart.

Acknowledgements

None

Sources of Funding

This work was supported by the British Heart Foundation (Programme grant RG/12/16/29939 to HW and CR) and the British Heart Foundation Centre of Research Excellence (Oxford, RE/13/1/30181). Y-FC was supported by a pump priming grant from the British Heart Foundation Centre of Excellence award to Oxford University (RE/08/004/23915 and RE/13/1/30181). MJD is funded by the Wellcome Trust (WT098519MA) and the Japan Society for the Promotion of Science (JSPS) international joint research promotion program at Osaka University.

Disclosures

None.

References

1. Maron BJ, Gardin JM, Flack JM, Gidding SS, Kurosaki TT and Bild DE. Prevalence of hypertrophic cardiomyopathy in a general population of young adults. Echocardiographic analysis of 4111 subjects in the CARDIA Study. Coronary Artery Risk Development in (Young) Adults. *Circulation*. 1995;92:785-9.
2. Watkins H, Ashrafian H and Redwood C. Inherited cardiomyopathies. *N Engl J Med*. 2011;364:1643-56.
3. Walsh R, Buchan R, Wilk A, John S, Felkin LE, Thomson KL, Chiaw TH, Loong CCW, Pua CJ, Raphael C, Prasad S, Barton PJ, Funke B, Watkins H, Ware JS and Cook SA. Defining the genetic architecture of hypertrophic cardiomyopathy: re-evaluating the role of non-sarcomeric genes. *Eur Heart J*. 2017;38:3461-3468.
4. Redwood CS, Moolman-Smook JC and Watkins H. Properties of mutant contractile proteins that cause hypertrophic cardiomyopathy. *Cardiovasc Res*. 1999;44:20-36.
5. Knollmann BC, Kirchhof P, Sirenko SG, Degen H, Greene AE, Schober T, Mackow JC, Fabritz L, Potter JD and Morad M. Familial hypertrophic cardiomyopathy-linked mutant troponin T causes stress-induced ventricular tachycardia and Ca2+-dependent action potential remodeling. *Circ Res*. 2003;92:428-36.
6. Spindler M, Saupe KW, Christe ME, Sweeney HL, Seidman CE, Seidman JG and Ingwall JS. Diastolic dysfunction and altered energetics in the alphaMHC403/+ mouse model of familial hypertrophic cardiomyopathy. *J Clin Invest*. 1998;101:1775-83.
7. Kobayashi T and Solaro RJ. Increased Ca2+-affinity of cardiac thin filaments reconstituted with cardiomyopathy-related mutant cardiac troponin I. *J Biol Chem*. 2006;12:13471-7.
8. Robinson P, Griffiths PJ, Watkins H and Redwood CS. Dilated and hypertrophic cardiomyopathy mutations in troponin and alpha-tropomyosin have opposing effects on the calcium affinity of cardiac thin filaments. *Circ Res*. 2007;101:1266-73.
9. Adhikari AS, Kooiker KB, Sarkar SS, Liu C, Bernstein D, Spudich JA and Ruppel KM. Early-Onset Hypertrophic Cardiomyopathy Mutations Significantly Increase the Velocity, Force, and Actin-Activated ATPase Activity of Human beta-Cardiac Myosin. *Cell Rep*. 2016;17:2857-2864.
10. Robinson P, Liu X, Sparrow A, Patel S, Zhang YH, Casadei B, Watkins H and Redwood C. Hypertrophic cardiomyopathy mutations increase myofilament Ca(2+) buffering, alter intracellular Ca(2+) handling, and stimulate Ca(2+)-dependent signaling. *J Biol Chem*. 2018;293:10487-10499.
11. Schober T, Huke S, Venkataraman R, Gryshchenko O, Kryshtal D, Hwang HS, Baudenbacher FJ and Knollmann BC. Myofilament Ca sensitization increases cytosolic Ca binding affinity, alters intracellular Ca homeostasis, and causes pause-dependent Ca-triggered arrhythmia. *Circ Res*. 2012;111:170-9.
12. Coppini R, Mazzoni L, Ferrantini C, Gentile F, Pioner JM, Laurino A, Santini L, Bargelli V, Rotellini M, Bartolucci G, Crocini C, Sacconi L, Tesi C, Belardinelli L, Tardiff J, Mugelli A, Olivotto I, Cerbai E and Poggesi C. Ranolazine Prevents Phenotype Development in a Mouse Model of Hypertrophic Cardiomyopathy. *Circ Heart Fail*. 2017;10:e003565.
13. Davis J, Davis LC, Correll RN, Makarewich CA, Schwanekamp JA, Moussavi-Harami F, Wang D, York AJ, Wu H, Houser SR, Seidman CE, Seidman JG, Regnier M, Metzger JM, Wu JC and Molkentin JD. A Tension-Based Model Distinguishes Hypertrophic versus Dilated Cardiomyopathy. *Cell*. 2016;165:1147-59.
14. Olivotto I, Cecchi F, Poggesi C and Yacoub MH. Developmental origins of hypertrophic cardiomyopathy phenotypes: a unifying hypothesis. *Nat Rev Cardiol*. 2009;6:317-21.
15. Crilley JG, Boehm EA, Blair E, Rajagopalan B, Blamire AM, Styles P, McKenna WJ, Ostman-Smith I, Clarke K and Watkins H. Hypertrophic cardiomyopathy due to sarcomeric gene mutations is characterized by impaired energy metabolism irrespective of the degree of hypertrophy. *J Am Coll Cardiol*. 2003;41:1776-82.
16. Grynkiewicz G, Poenie M and Tsien RY. A new generation of Ca2+ indicators with greatly improved fluorescence properties. *J Biol Chem*. 1985;260:3440-50.

17. Kaestner L, Scholz A, Tian Q, Ruppenthal S, Tabellion W, Wiesen K, Katus HA, Muller OJ, Kotlikoff MI and Lipp P. Genetically encoded Ca2+ indicators in cardiac myocytes. *Circ Res*. 2014;114:1623-39.
18. Ljubojevic S, Walther S, Asgarzoei M, Sedej S, Pieske B and Kockskamper J. In situ calibration of nucleoplasmic versus cytoplasmic Ca(2)+ concentration in adult cardiomyocytes. *Biophys J*. 2011;100:2356-66.
19. Broyles CN, Robinson P and Daniels MJ. Fluorescent, Bioluminescent, and Optogenetic Approaches to Study Excitable Physiology in the Single Cardiomyocyte. *Cells*. 2018;7:51.
20. Trafford AW, Diaz ME and Eisner DA. A novel, rapid and reversible method to measure Ca buffering and time-course of total sarcoplasmic reticulum Ca content in cardiac ventricular myocytes. *Pflugers Arch*. 1999;437:501-3.
21. Akerboom J, Carreras Calderon N, Tian L, Wabnig S, Prigge M, Tolo J, Gordus A, Orger MB, Severi KE, Macklin JJ, Patel R, Pulver SR, Wardill TJ, Fischer E, Schuler C, Chen TW, Sarkisyan KS, Marvin JS, Bargmann CI, Kim DS, Kugler S, Lagnado L, Hegemann P, Gottschalk A, Schreiter ER and Looger LL. Genetically encoded calcium indicators for multi-color neural activity imaging and combination with optogenetics. *Front Mol Neurosci*. 2013;6:2.
22. Spudich JA. Hypertrophic and dilated cardiomyopathy: four decades of basic research on muscle lead to potential therapeutic approaches to these devastating genetic diseases. *Biophys J*. 2014;106:1236-49.
23. Paul DM, Morris EP, Kensler RW and Squire JM. Structure and orientation of troponin in the thin filament. *J Biol Chem*. 2009;284:15007-15.
24. Surdo NC, Berrera M, Koschinski A, Brescia M, Machado MR, Carr C, Wright P, Gorelik J, Morotti S, Grandi E, Bers DM, Pantano S and Zaccolo M. FRET biosensor uncovers cAMP nano-domains at beta-adrenergic targets that dictate precise tuning of cardiac contractility. *Nat Commun*. 2017;8:15031.
25. Mank M, Reiff DF, Heim N, Friedrich MW, Borst A and Griesbeck O. A FRET-based calcium biosensor with fast signal kinetics and high fluorescence change. *Biophys J*. 2006;90:1790-6.
26. Mank M, Santos AF, Direnberger S, Mrsic-Flogel TD, Hofer SB, Stein V, Hendel T, Reiff DF, Levelt C, Borst A, Bonhoeffer T, Hubener M and Griesbeck O. A genetically encoded calcium indicator for chronic in vivo two-photon imaging. *Nat Methods*. 2008;5:805-11.
27. Henderson MJ, Baldwin HA, Werley CA, Boccardo S, Whitaker LR, Yan X, Holt GT, Schreiter ER, Looger LL, Cohen AE, Kim DS and Harvey BK. A Low Affinity GCaMP3 Variant (GCaMPer) for Imaging the Endoplasmic Reticulum Calcium Store. *PLoS One*. 2015;10:e0139273.
28. Despa S, Shui B, Bossuyt J, Lang D, Kotlikoff MI and Bers DM. Junctional cleft [Ca(2)(+)]i measurements using novel cleft-targeted Ca(2)(+) sensors. *Circ Res*. 2014;115:339-47.
29. Pollesello P, Papp Z and Papp JG. Calcium sensitizers: What have we learned over the last 25 years? *Int J Cardiol*. 2016;203:543-8.
30. Green EM, Wakimoto H, Anderson RL, Evanchik MJ, Gorham JM, Harrison BC, Henze M, Kawas R, Oslob JD, Rodriguez HM, Song Y, Wan W, Leinwand LA, Spudich JA, McDowell RS, Seidman JG and Seidman CE. A small-molecule inhibitor of sarcomere contractility suppresses hypertrophic cardiomyopathy in mice. *Science*. 2016;351:617-21.
31. Papp Z, Edes I, Fruhwald S, De Hert SG, Salmenpera M, Leppikangas H, Mebazaa A, Landoni G, Grossini E, Caimmi P, Morelli A, Guarracino F, Schwinger RH, Meyer S, Algotsson L, Wikstrom BG, Jorgensen K, Filippatos G, Parissis JT, Gonzalez MJ, Parkhomenko A, Yilmaz MB, Kivikko M, Pollesello P and Follath F. Levosimendan: molecular mechanisms and clinical implications: consensus of experts on the mechanisms of action of levosimendan. *Int J Cardiol*. 2012;159:82-7.
32. Watkins H, McKenna WJ, Thierfelder L, Suk HJ, Anan R, O'Donoghue A, Spirito P, Matsumori A, Moravec CS, Seidman JG and et al. Mutations in the genes for cardiac troponin T and alpha-tropomyosin in hypertrophic cardiomyopathy. *N Engl J Med*. 1995;332:1058-64.

33. Thierfelder L, Watkins H, MacRae C, Lamas R, McKenna W, Vosberg HP, Seidman JG and Seidman CE. Alpha-tropomyosin and cardiac troponin T mutations cause familial hypertrophic cardiomyopathy: a disease of the sarcomere. *Cell*. 1994;77:701-12.
34. Elliott K, Watkins H and Redwood CS. Altered regulatory properties of human cardiac troponin I mutants that cause hypertrophic cardiomyopathy. *J Biol Chem*. 2000;275:22069-74.
35. Kimura A, Harada H, Park JE, Nishi H, Satoh M, Takahashi M, Hiroi S, Sasaoka T, Ohbuchi N, Nakamura T, Koyanagi T, Hwang TH, Choo JA, Chung KS, Hasegawa A, Nagai R, Okazaki O, Nakamura H, Matsuzaki M, Sakamoto T, Toshima H, Koga Y, Imaizumi T and Sasazuki T. Mutations in the cardiac troponin I gene associated with hypertrophic cardiomyopathy. *Nat Genet*. 1997;16:379-82.
36. Michele DE, Albayya FP and Metzger JM. Direct, convergent hypersensitivity of calcium-activated force generation produced by hypertrophic cardiomyopathy mutant alpha-tropomyosins in adult cardiac myocytes. *Nat Med*. 1999;5:1413-7.
37. Ellingsen O, Davidoff AJ, Prasad SK, Berger HJ, Springhorn JP, Marsh JD, Kelly RA and Smith TW. Adult rat ventricular myocytes cultured in defined medium: phenotype and electromechanical function. *Am J Physiol*. 1993;265:H747-54.
38. Robinson P, Mirza M, Knott A, Abdulrazzak H, Willott R, Marston S, Watkins H and Redwood C. Alterations in thin filament regulation induced by a human cardiac troponin T mutant that causes dilated cardiomyopathy are distinct from those induced by troponin T mutants that cause hypertrophic cardiomyopathy. *J Biol Chem*. 2002;277:40710-6.
39. Pardee JD and Spudich JA. Purification of muscle actin. *Methods Cell Biol*. 1982;24:271-89.
40. Weeds AG and Taylor RS. Separation of subfragment-1 isoenzymes from rabbit skeletal muscle myosin. *Nature*. 1975;257:54-6.
41. Zhao Y, Araki S, Wu J, Teramoto T, Chang YF, Nakano M, Abdelfattah AS, Fujiwara M, Ishihara T, Nagai T and Campbell RE. An expanded palette of genetically encoded Ca(2)(+) indicators. *Science*. 2011;333:1888-91.
42. Simon JN, Chowdhury SA, Warren CM, Sadayappan S, Wieczorek DF, Solaro RJ and Wolska BM. Ceramide-mediated depression in cardiomyocyte contractility through PKC activation and modulation of myofilament protein phosphorylation. *Basic Res Cardiol*. 2014;109:445.
43. Chang YF, Broyles CN, Brook FA, Davies MJ, Turtle CW, Nagai T and Daniels MJ. Non-invasive phenotyping and drug testing in single cardiomyocytes or beta-cells by calcium imaging and optogenetics. *PLoS One*. 2017;12:e0174181.
44. Hilliard FA, Steele DS, Laver D, Yang Z, Le Marchand SJ, Chopra N, Piston DW, Huke S and Knollmann BC. Flecainide inhibits arrhythmogenic Ca2+ waves by open state block of ryanodine receptor Ca2+ release channels and reduction of Ca2+ spark mass. *J Mol Cell Cardiol*. 2010;48:293-301.
45. Mosqueira D, Mannhardt I, Bhagwan JR, Lis-Slimak K, Katili P, Scott E, Hassan M, Prondzynski M, Harmer SC, Tinker A, Smith JGW, Carrier L, Williams PM, Gaffney D, Eschenhagen T, Hansen A and Denning C. CRISPR/Cas9 editing in human pluripotent stem cell-cardiomyocytes highlights arrhythmias, hypocontractility, and energy depletion as potential therapeutic targets for hypertrophic cardiomyopathy. *Eur Heart J*. 2018;39:3879-3892.
46. Fabiato A and Fabiato F. Effects of pH on the myofilaments and the sarcoplasmic reticulum of skinned cells from cardiace and skeletal muscles. *J Physiol*. 1978;276:233-55.
47. Griffiths EJ. Calcium handling and cell contraction in rat cardiomyocytes depleted of intracellular magnesium. *Cardiovasc Res*. 2000;47:116-23.
48. Malik FI, Hartman JJ, Elias KA, Morgan BP, Rodriguez H, Brejc K, Anderson RL, Sueoka SH, Lee KH, Finer JT, Sakowicz R, Baliga R, Cox DR, Garard M, Godinez G, Kawas R, Kraynack E, Lenzi D, Lu PP, Muci A, Niu C, Qian X, Pierce DW, Pokrovskii M, Suehiro I, Sylvester S, Tochimoto T, Valdez C, Wang W, Katori T, Kass DA, Shen YT, Vatner SF and Morgans DJ. Cardiac myosin activation: a potential therapeutic approach for systolic heart failure. *Science*. 2011;331:1439-43.

49. Orstavik O, Ata SH, Riise J, Dahl CP, Andersen GO, Levy FO, Skomedal T, Osnes JB and Qvigstad E. Inhibition of phosphodiesterase-3 by levosimendan is sufficient to account for its inotropic effect in failing human heart. *Br J Pharmacol*. 2014;171:5169-81.
50. Kopustinskiene DM, Pollesello P and Saris NE. Levosimendan is a mitochondrial K(ATP) channel opener. *Eur J Pharmacol*. 2001;428:311-4.
51. Mosqueira D, Mannhardt I, Bhagwan JR, Lis-Slimak K, Katili P, Scott E, Hassan M, Prondzynski M, Harmer SC, Tinker A, Smith JGW, Carrier L, Williams PM, Gaffney D, Eschenhagen T, Hansen A and Denning C. CRISPR/Cas9 editing in human pluripotent stem cell-cardiomyocytes highlights arrhythmias, hypocontractility, and energy depletion as potential therapeutic targets for hypertrophic cardiomyopathy. *Eur Heart J*. 2018.
52. Fatkin D, McConnell BK, Mudd JO, Semsarian C, Moskowitz IG, Schoen FJ, Giewat M, Seidman CE and Seidman JG. An abnormal Ca(2+) response in mutant sarcomere protein-mediated familial hypertrophic cardiomyopathy. *J Clin Invest*. 2000;106:1351-9.
53. Tardiff JC. The Role of Calcium/Calmodulin-Dependent Protein Kinase II Activation in Hypertrophic Cardiomyopathy. *Circulation*. 2016;134:1749-1751.
54. Smith NA, Kress BT, Lu Y, Chandler-Militello D, Benraiss A and Nedergaard M. Fluorescent Ca(2+) indicators directly inhibit the Na,K-ATPase and disrupt cellular functions. *Sci Signal*. 2018;11:eaal2039.

Figure 1. The effect of GFP conjugation to the N and C terminus of troponin subunits on myofilament function. Myofilament function was assessed using in vitro actin activated acto-myosin S1 ATPase assays. Control (unconjugated) troponin complexes (grey lines) were compared pairwise to troponin complex reconstituted with subunits conjugated to the N or the C terminus of GFP as illustrated (red lines). n=3-5 error bars are ± SEM.

Figure 2. Fluorescent and contractile properties of RGECO, RGECO-TnT and RGECO-TnI. Steady state fluorescence excitation, emission spectra (peak excitation (Ex) = 564nm) / peak emission (Em) = 581nm) were obtained at pCa4.5 and subtracted from paired spectra at pCa8.5 for purified recombinant RGECO (**A**), RGECO-TnT (**B**) and RGECO-TnI (**C**). Sarcomere shortening during electrical pacing (0.5Hz) of isolated adult cardiomyocytes was used to test cardiac contractile function in non-transduced and either RGECO, RGECO-TnT or RGECO-TnI transduced GPCMs by measurement of the sarcomeric length during contraction (n=33-52) (**D**) or by fractional shortening (**E**).

Figure 3. Characterisation of RGECO, RGECO-TnT and RGECO-TnI in GPCMs. Adenovirally expressed RGECO-TnT and RGECO-TnI (red in the merged images) localises to the I band in confocal microscopy of GPCMs, whilst RGECO shows diffuse staining (n=4) (**A**); Z-disks are revealed by α-actinin staining (green in the merged images). Scale bar = 5μm. Intensity profile plots spanning two sarcomeres, α-actinin (green line) labels the z-disc, DsRed (red) labels the Ca^{2+} sensors. Western blot analysis of GPCMs transduced with RGECO-TnT (**B**) or RGECO-TnI (**C**) indicates that 54.3±5.5% (n=5)/58.7±11.0% (n=4), respectively, of Troponin is composed of RGECO conjugated Troponin. Raw Ca^{2+} transients of paced GPCMs transduced with RGECO-TnT (**D**) or RGECO-TnI (**E**). Averaged Ca^{2+} transients of 0.5Hz paced GPCMs transduced with RGECO, RGECO-TnT or RGECO-TnI (**F**) was used to compare Ca^{2+} transients between cytoplasmic RGECO and myofilament specific RGECO-TnT and RGECO-TnI.

Figure 4. The effects of MYK-461 on Ca^{2+} transient measurements in GPCMs with RGECO, RGECO-TnT or RGECO-TnI. Averaged Ca^{2+} transients of 0.5 Hz paced GPCMs transduced with RGECO, RGECO-TnT or RGECO-TnI was used to compare the effects of 250nmol/L MYK-461 (**A**). Each comparison is made in paired experiments between drug treated (solid lines) and DMSO control treated (dashed lines) for RGECO infected (red), RGECO-TnT infected (purple) and RGECO-TnI infected (blue) cells. Dot plots for all extracted parameters are plotted in **(B)** (n=43-82 cells from n=3 isolations). Lines are median average and error bars are interquartile range, **= $p<0.01$ and ***= $p<0.001$ using an unpaired Mann-Whitney test comparing untreated to treated cells.

Figure 5. The effects of omecamtiv mecarbil on Ca^{2+} transient measurements in GPCMs with RGECO, RGECO-TnT or RGECO-TnI. Averaged Ca^{2+} transients of 0.5Hz paced GPCMs transduced with RGECO, RGECO-TnT or RGECO-TnI was used to compare the effects 200nmol/L omecamtiv mecarbil (**A**). Each comparison is made in paired experiments between drug treated (solid lines) and DMSO control treated (dashed lines) for RGECO infected (red), RGECO-TnT infected (purple) and RGECO-TnI infected (blue) cells Dot plots for all extracted parameters are plotted in **(B)** (n=42-75 cells from n=3 isolations). Lines are median average and error bars are interquartile range, all groups were not significant using an unpaired Mann-Whitney test comparing untreated to treated cells.

Figure 6. The effects of levosimendan on Ca^{2+} transient measurements in GPCMs with RGECO, RGECO-TnT or RGECO-TnI. Averaged Ca^{2+} transients of 0.5Hz paced GPCMs transduced with RGECO, RGECO-TnT or RGECO-TnI was used to compare the effects 10μmol/L levosimendan (**A**). Each comparison is made in paired experiments between drug treated (solid lines) and DMSO control treated (dashed lines) for RGECO infected (red), RGECO-TnT infected (purple) and RGECO-TnI

infected (blue) cells. Dot plots for all extracted parameters are plotted in **(B)** (n=71-83 cells from n=3 isolations). Lines are median average and error bars are interquartile range, *=p<0.05 **= p<0.01 and ***= p<0.001 using an unpaired Mann-Whitney test comparing untreated to treated cells.

Figure 7. Cytoplasmic and myofilament localised Ca^{2+} transients with adenovirally transduced cTnT R92Q and cTnI R145G. Averaged Ca^{2+} transients of 0.5Hz paced GPCMs transduced with RGECO (**A** and **B**) or RGECO-TnI/RGECO-TnT (**C** and **D**) was used to compare Ca^{2+} transient effects between GPCMs transduced with either WT cTnT/cTnT R92Q (**A** and **C**), or WT cTnI/cTnI R145G (**B** and **D**). Peak amplitude ratio (**E**) and Δvalues for time to 50% binding (On) (**F**) and 50% release (Off) (**G)** are plotted including significance and labelled cytoplasmic (c) and myofilament (m) (n=94-124 cells from n=3 isolations). Error bars are SD, **= p<0.01 and ***= p<0.001 using a Mann-Whitney test comparing WT troponin to mutant troponin transduced cells.

Novelty and Significance

What is known?

● Hypertrophic cardiomyopathy (HCM) mutations and small molecule modulators of contractility alter how the cardiomyocyte handles calcium.

● Historical methods to measure calcium at the myofilament are indirect because the chemical calcium dyes commonly used to visualise calcium are not possible to confine to subcellular regions.

● An additional limitation of using chemical calcium dyes in this context is their reported attenuation of contractility.

What new information does this article contribute?

● Calcium sensitive proteins, here we use RGECO, can be fused to two components of the thin filament (troponin I and troponin T) without adversely affecting the indicator, or native protein function, allowing calcium measurement from the sarcomere directly.

● We find that in spite of their size and calcium binding, amino terminal fusions are well tolerated and do not alter contractility biochemically or in intact cells.

● GECIs localised to the sarcomere detect changes to calcium amplitude or kinetics conferred by small molecules and HCM mutations that were not seen by traditional chemical calcium dyes or unrestricted GECIs that distribute throughout the cell.

We apply the virally delivered genetically encoded calcium indicators RGECO to measure beat-to-beat calcium transients in cardiomyocytes. By direct fusion to troponin I or troponin T, we have localised RGECO to measure calcium cycling within the contractile apparatus, where calcium is the master regulator of force production. Small molecule regulators of contractility (MYK-461, omecamtiv mecarbil and levosimendan) exert subtle changes to calcium at the myofilament which are more easily detected by these indicators working without the background noise coming from the whole cell. We find these tools increase our understanding of the mechanism by which HCM causing mutations alter microdomain calcium handling to drive disease state remodelling. Importantly the kinetic changes in contractility that arise in response to disease causing mutation are now mirrored by protein based calcium indicators. Overall, our work has developed novel tools to study myofilament domain calcium directly without several of the limitations encountered in previous strategies. We hope this study will inform deeper mechanistic understanding of contractile aspects of cardiovascular disease and lead to broader uptake of genetically encoded indicators to study cardiovascular physiology.

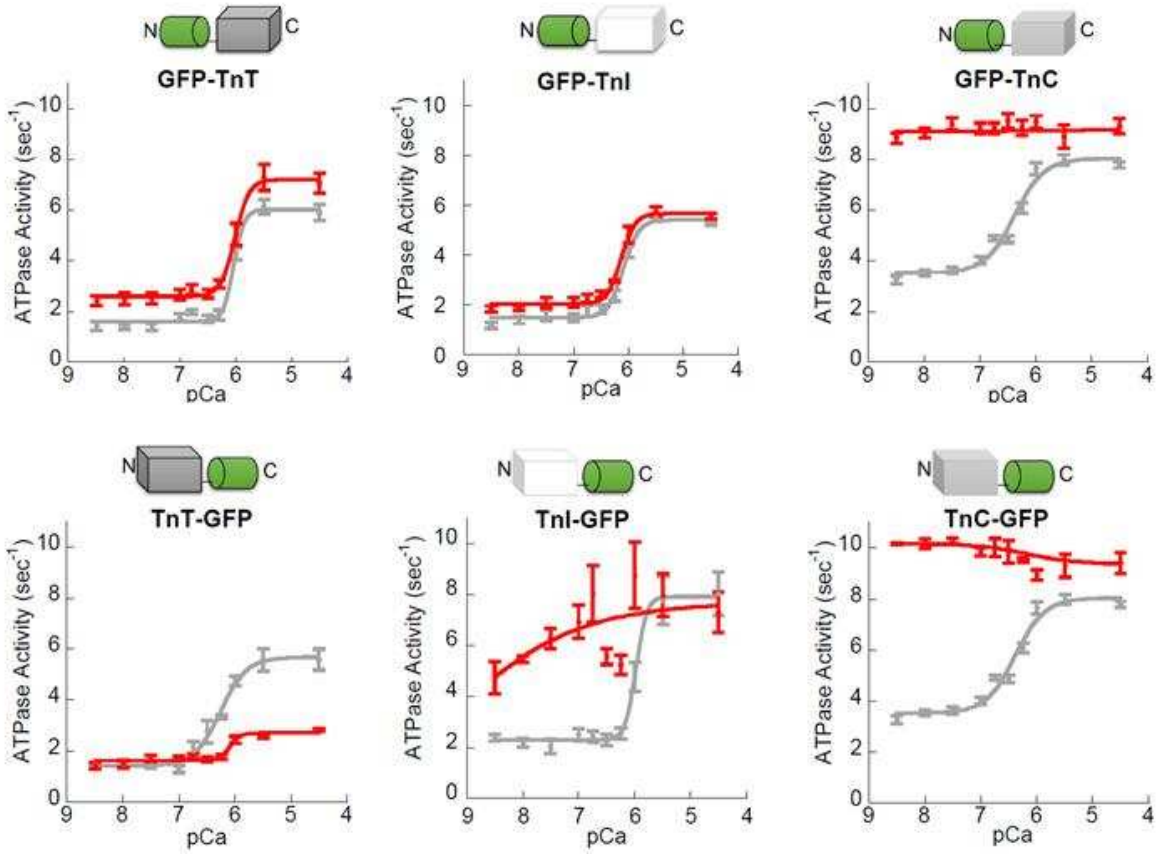
N
C
GFP-TnT
GFP-TnI
GFP-TnC
TnT-GFP
TnI-GFP
TnC-GFP
ATPase Activity (sec-1)
pCa
0
2
4
6
8
10
9
8
7
6
5
4

Figure 1

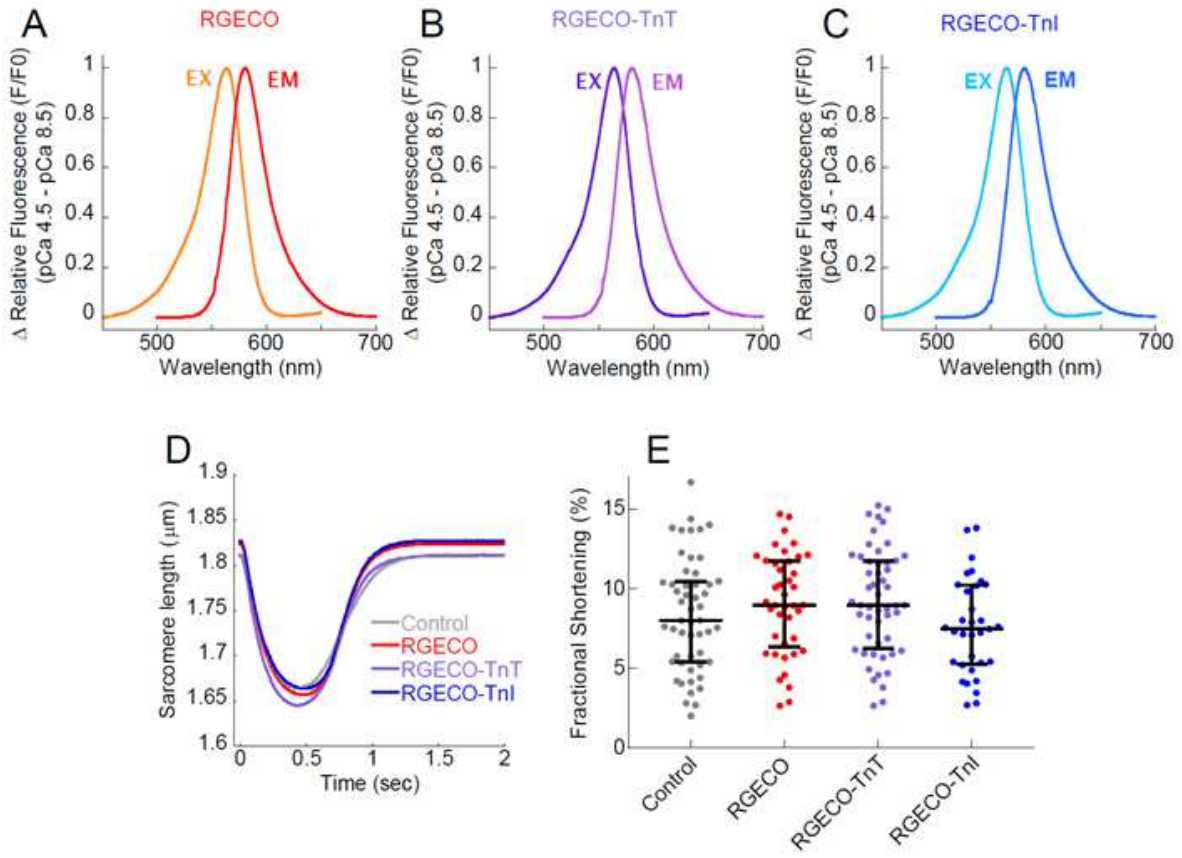
A
RGECO
EX
EM
Δ Relative Fluorescence (F/F0)
(pCa 4.5 - pCa 8.5)
Wavelength (nm)
B
RGECO-TnT
C
RGECO-TnI
D
Sarcomere length (μm)
Time (sec)
Control
RGECO
RGECO-TnT
RGECO-TnI
E
Fractional Shortening (%)

Figure 2

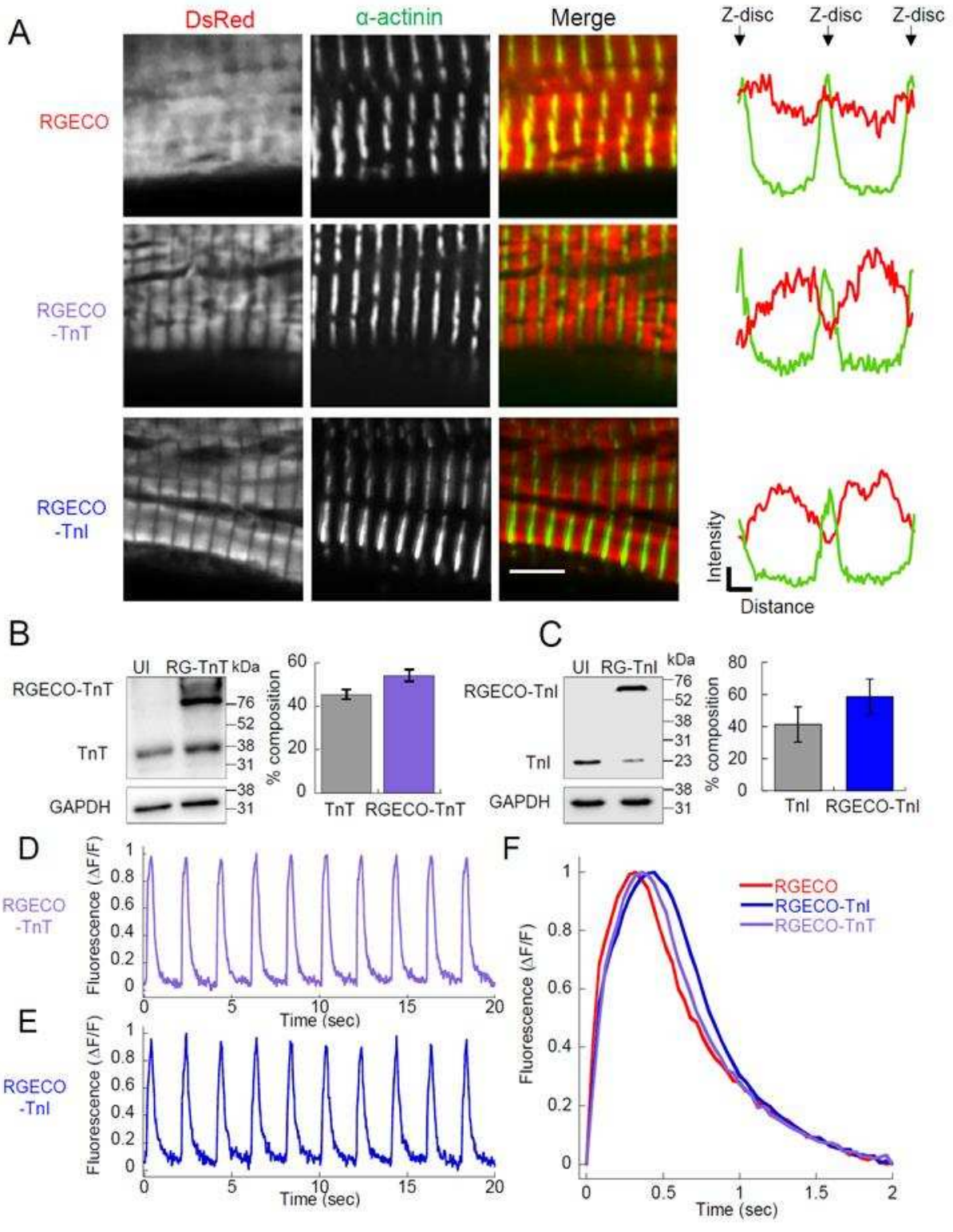
A
DsRed
α-actinin
Merge
Z-disc
Z-disc
Z-disc
RGECO
RGECO -TnT
RGECO -TnI
Intensity
Distance
B
UI
RG-TnT
kDa
RGECO-TnT
TnT
GAPDH
76
52
38
31
38
31
% composition
60
40
20
0
TnT
RGECO-TnT
C
UI
RG-TnI
kDa
RGECO-TnI
TnI
GAPDH
76
52
38
31
23
38
31
% composition
80
60
40
20
0
TnI
RGECO-TnI
D
RGECO -TnT
Fluorescence (ΔF/F)
Time (sec)
E
RGECO -TnI
Fluorescence (ΔF/F)
Time (sec)
F
RGECO
RGECO-TnI
RGECO-TnT
Fluorescence (ΔF/F)
Time (sec)

Figure 3

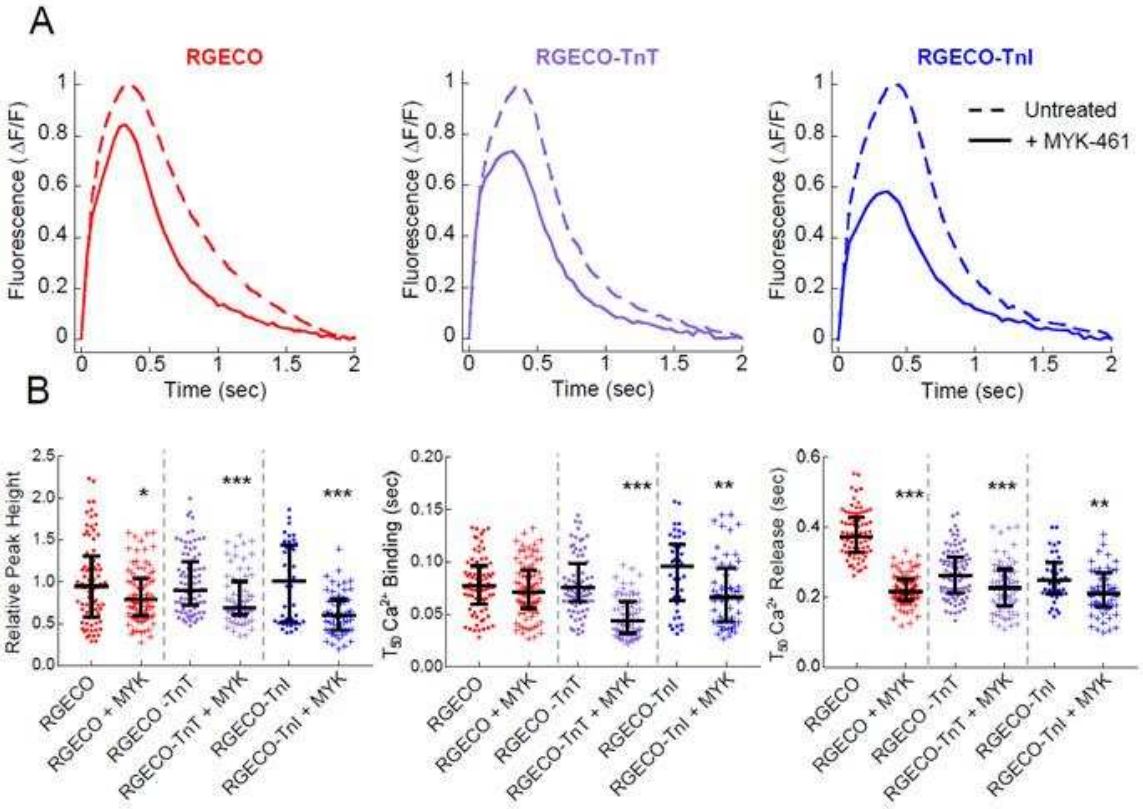
A
RGECO
RGECO-TnT
RGECO-TnI
Fluorescence (ΔF/F)
Time (sec)
Untreated
+ MYK-461
B
Relative Peak Height
T50 Ca2+ Binding (sec)
T90 Ca2+ Release (sec)
RGECO
RGECO + MYK
RGECO -TnT
RGECO-TnT + MYK
RGECO-TnI
RGECO-TnI + MYK

Figure 4

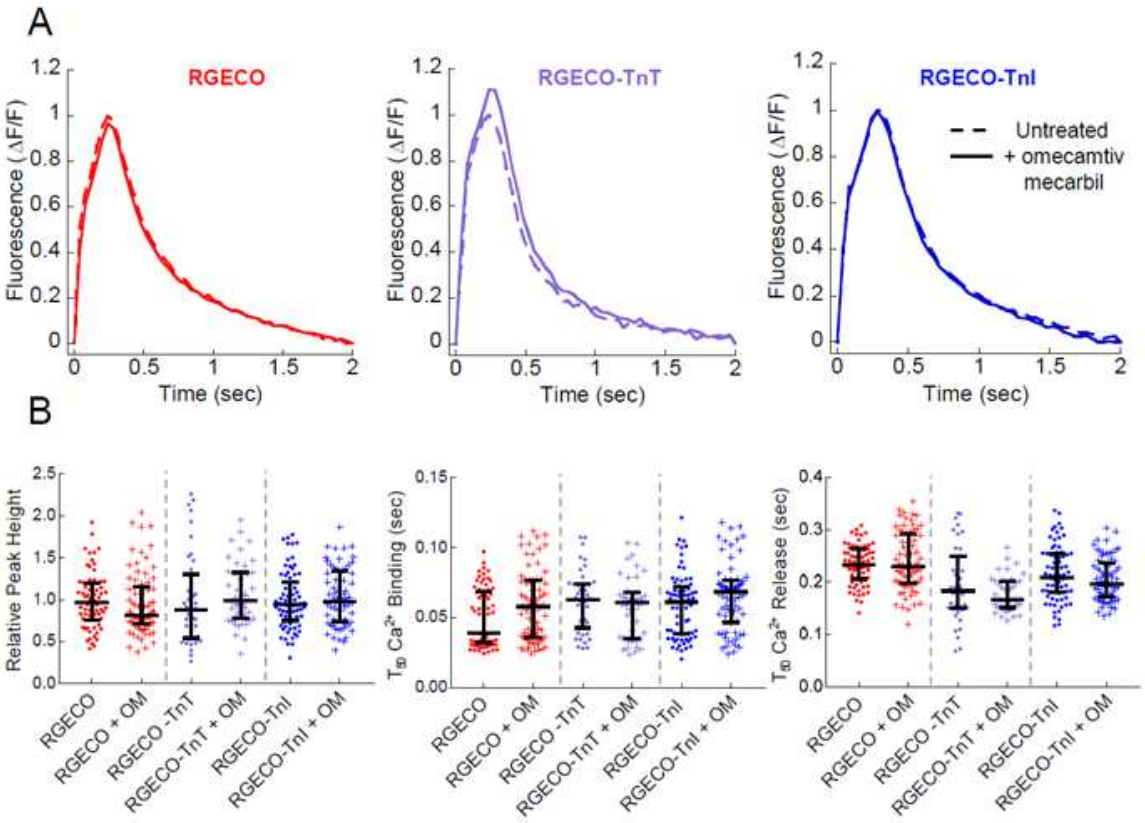
A
RGECO
RGECO-TnT
RGECO-TnI
Fluorescence (ΔF/F)
Time (sec)
Untreated
+ omecamtiv mecarbil
B
Relative Peak Height
T50 Ca2+ Binding (sec)
T50 Ca2+ Release (sec)
RGECO
RGECO + OM
RGECO -TnT
RGECO-TnT + OM
RGECO-TnI
RGECO-TnI + OM

Figure 5

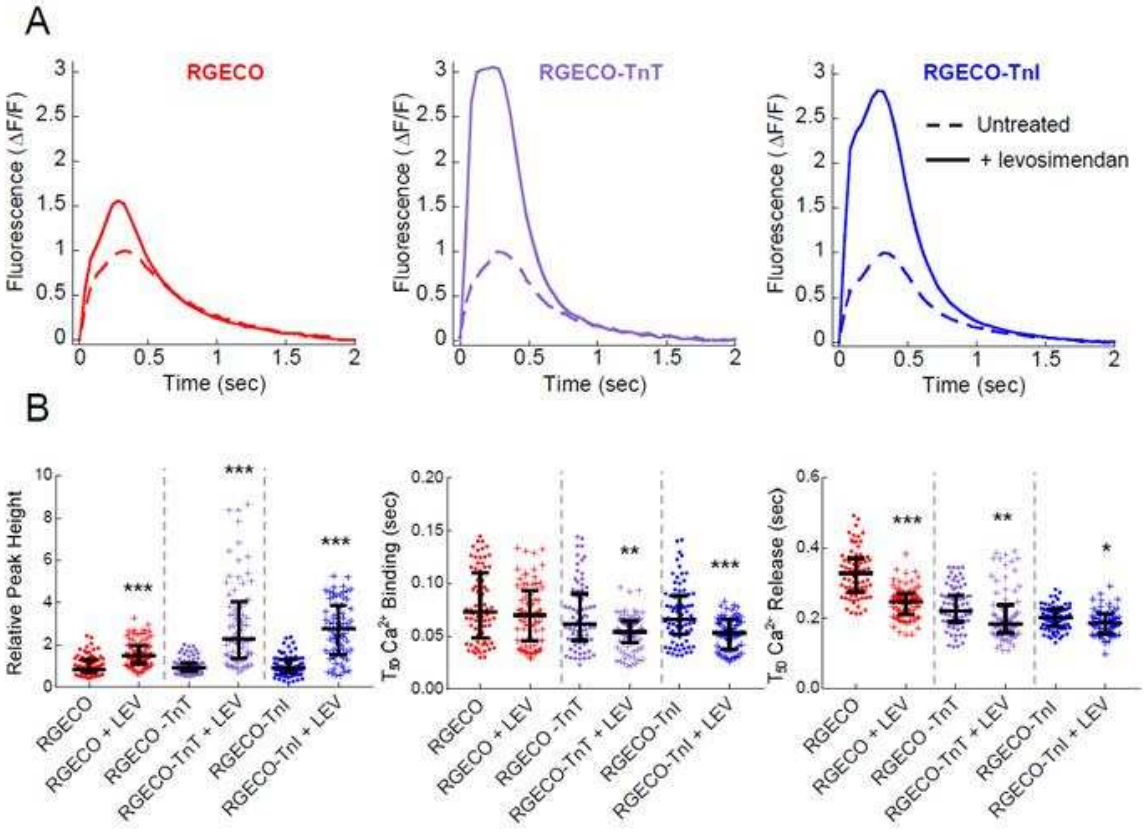
A
RGECO
RGECO-TnT
RGECO-TnI
Untreated
+ levosimendan
Fluorescence (ΔF/F)
Time (sec)
B
Relative Peak Height
T50 Ca2+ Binding (sec)
T50 Ca2+ Release (sec)
RGECO
RGECO + LEV
RGECO -TnT
RGECO-TnT + LEV
RGECO-TnI
RGECO-TnI + LEV

Figure 6

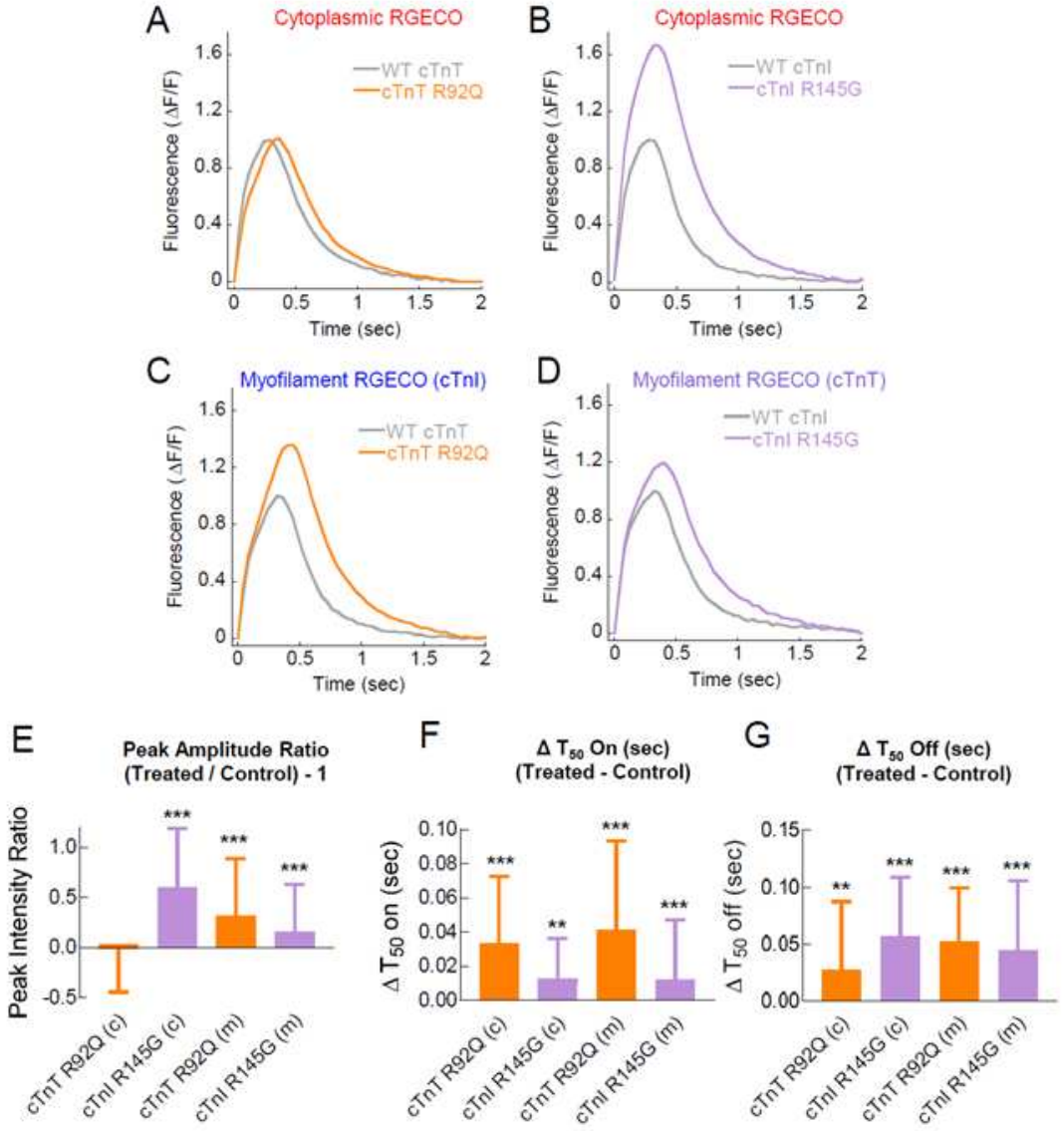
A
Cytoplasmic RGECO
WT cTnT
cTnT R92Q
Fluorescence (ΔF/F)
Time (sec)
B
Cytoplasmic RGECO
WT cTnI
cTnI R145G
C
Myofilament RGECO (cTnI)
D
Myofilament RGECO (cTnT)
E
Peak Amplitude Ratio
(Treated / Control) - 1
Peak Intensity Ratio
F
Δ T50 On (sec)
(Treated - Control)
G
Δ T50 Off (sec)
(Treated - Control)
cTnT R92Q (c)
cTnI R145G (c)
cTnT R92Q (m)
cTnI R145G (m)

Figure 7

SUPPLEMENTAL MATERIAL

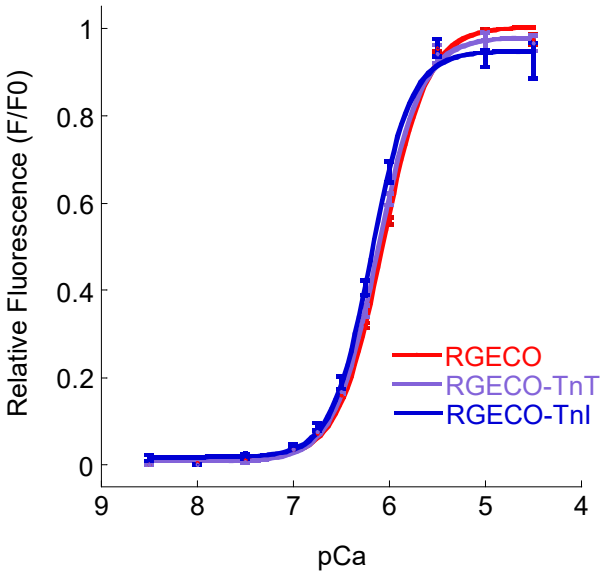

Online Figure I. Ca^{2+} binding affinity plot of RGECO, RGECO-TnT and RGECO-TnI. The steady state Ca^{2+} binding affinity of purified recombinant RGECO (red lines) RGECO-TnT (purple lines) and RGECO-TnI (blue lines) was assessed by analysis of the fluorescence/pCa relationship at 37 °C, 1.3 mM $MgCl_2$ and pH 7.3 (n=4).

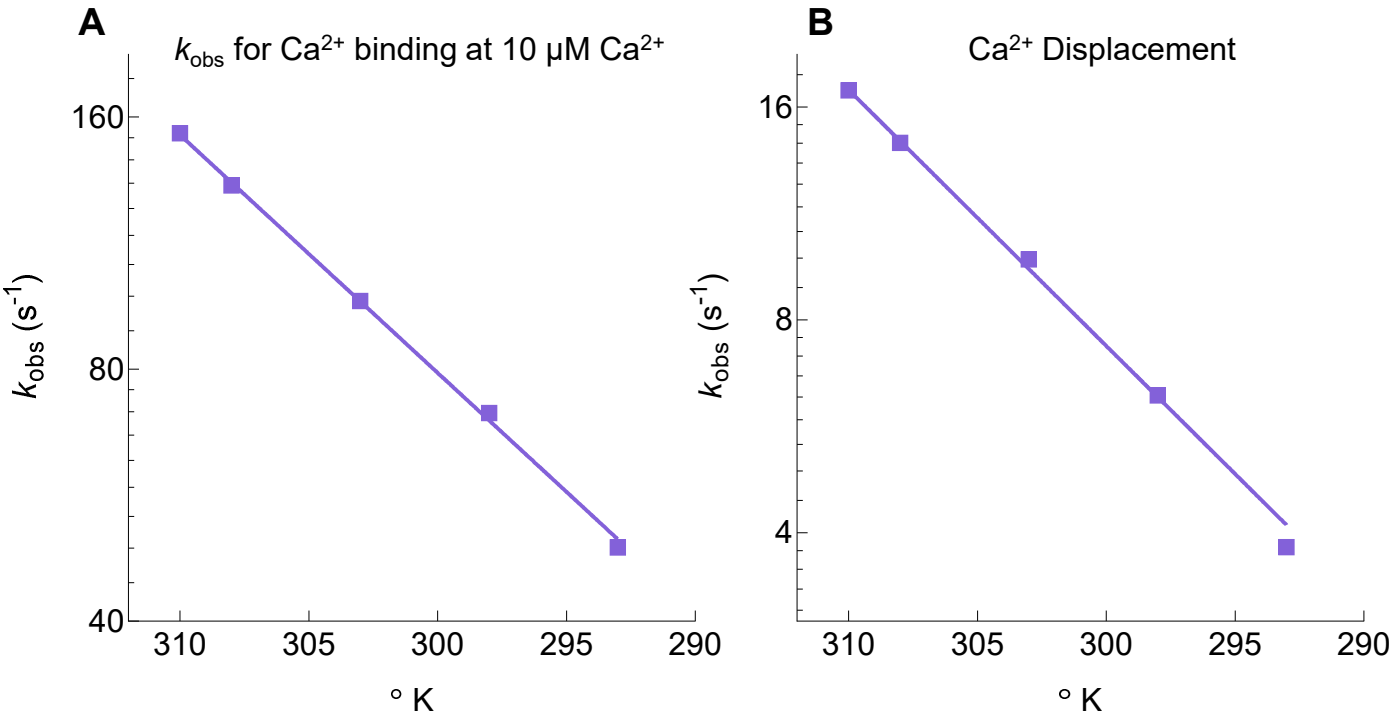

C

	k_{off}/s^{-1}		k_{on}/s^{-1}	
Temp (°C)	**25**	**37**	**25**	**37**
RGECO-TnT	6.3	16.9	70.9	167.0

Online Figure II. Kinetic determination of k_{on} and k_{off} for RGECO-TnT by stopped flow. Arrhenius plots of the observed rate constant of Ca^{2+} binding **(A)** and Ca^{2+} release rate constant **(B)** as determined by stopped flow measurement of 0.125 µM purified RGECO-TnT protein. Data for room (25 °C) and body (37 °C) temperature are shown in **(C).**

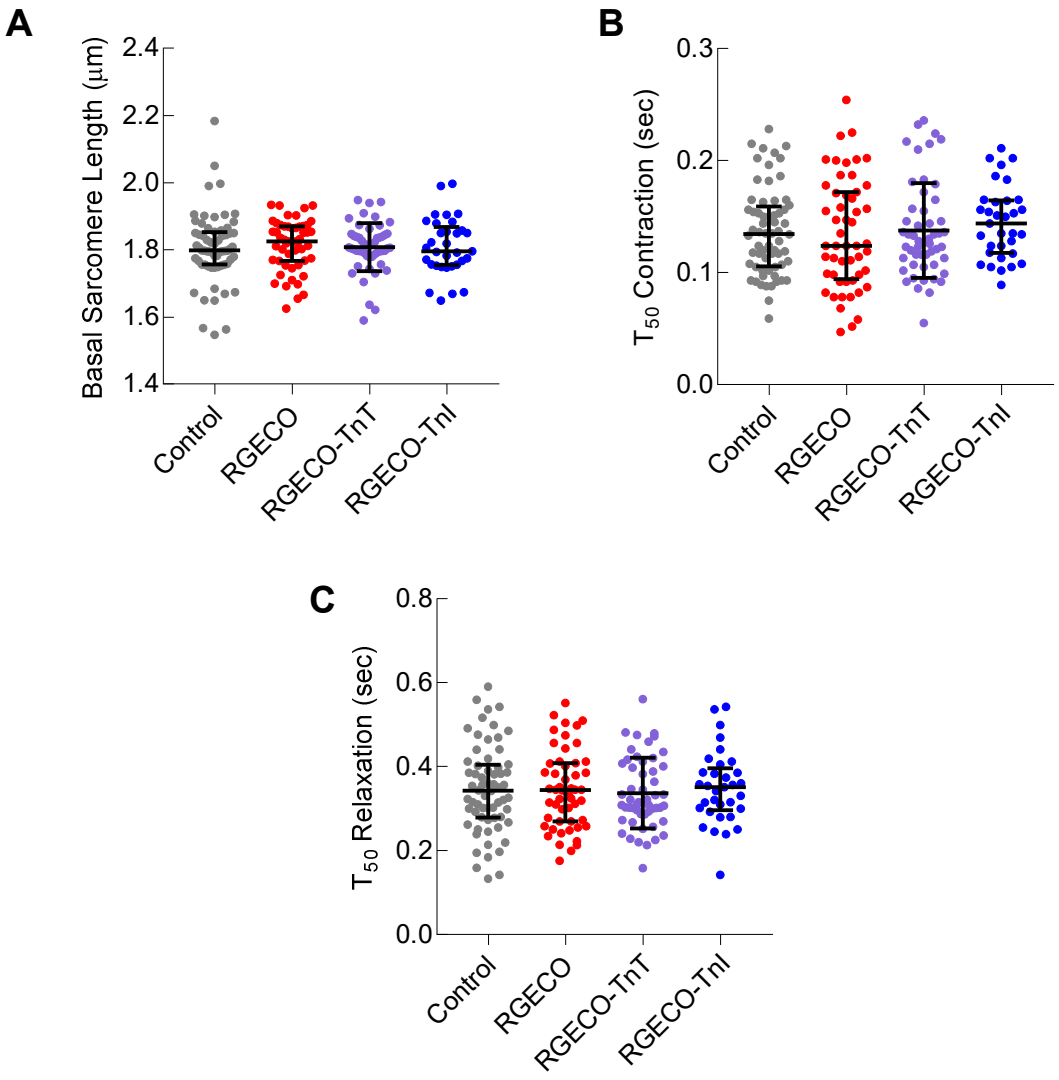

Online Figure III. Contractile properties of RGECO, RGECO-TnT and RGECO-TnI. Contractile parameters during electrical paced (0.5 Hz) of isolated adult cardiomyocytes transduced and either RGECO, RGECO-TnT or RGECO-TnI showing no change in basal sarcomere length (**A**), time to 50% contraction (**B**) or time to 50% relaxation (**C**) (n=33-64 cells from n=3 isolations).

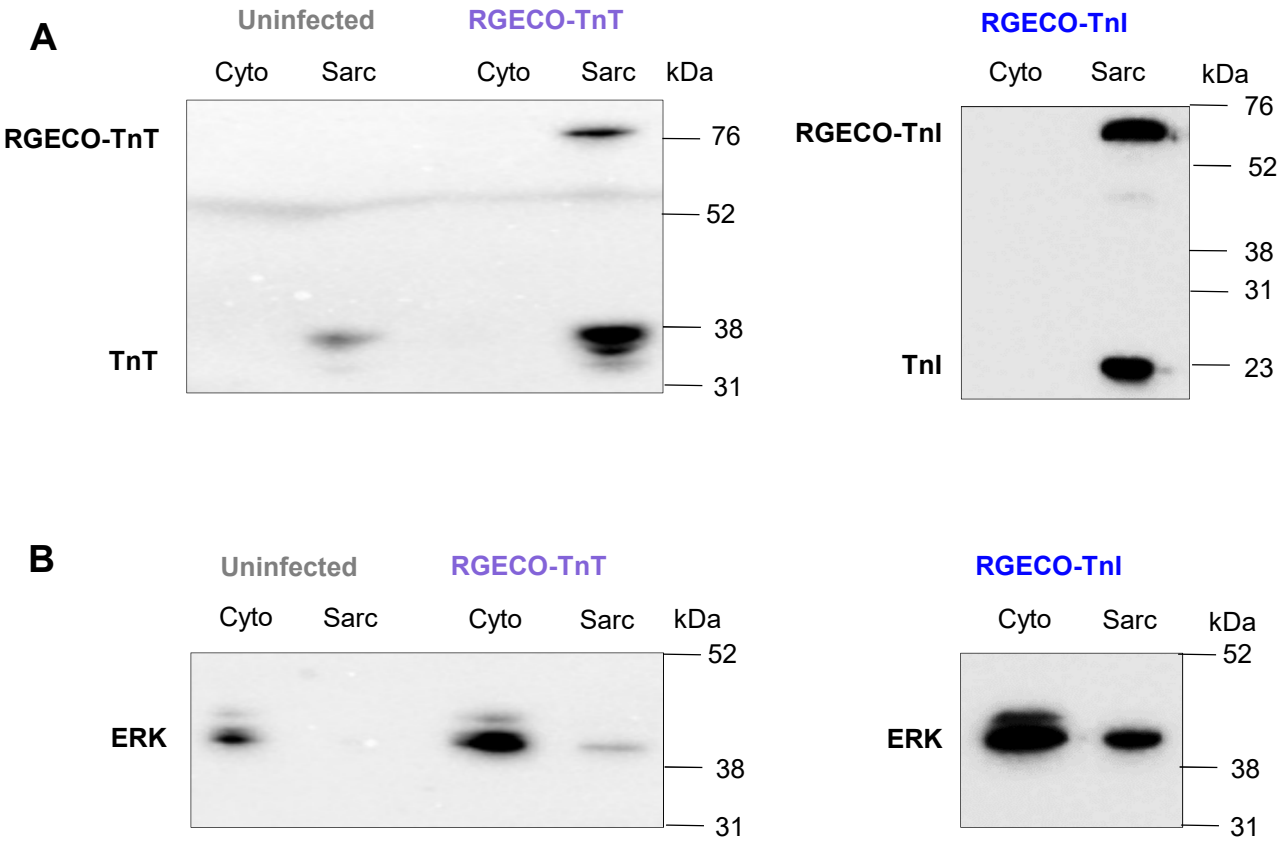

Online Figure IV. Subcellular fractionation of GPCMs expressing RGECO-TnT and RGECO-TnI. The relative subcellular incorporation of RGECO-TnT or RGECO-TnI was assessed by subcellular fractionation of GPCMs 48 hours after adenoviral infection. Western blots using anti-cTnT or anti-cTnI gave an endogenous band and a conjugate band on the sarcomeric fraction (sarc) **(A)**. Re-probing with the predominantly cytoplasmic marker anti-ERK showed that subcellular fractionation was of high fidelity **(B)**.

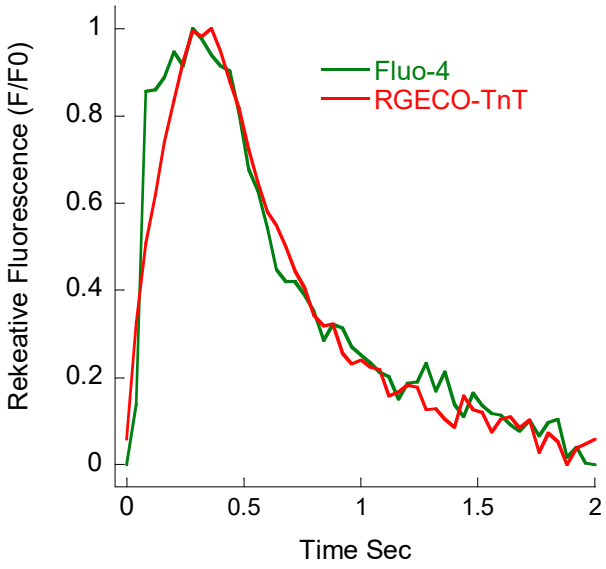

	Fluo-4	RGECO-TnT
T_{50} on (sec)	0.059±0.003	0.088±0.004 *
T_{50} off (sec)	0.418±0.026	0.316±0.038 *

Online Figure V. The on and off rates of Ca^{2+} transients measured with Fluo-4 are significantly different to RGECO-TnT in simultaneous measurements if dye and sensor in the same cell. Fluorescence measurements taken from cells loaded with 0.5 µmol/L Fluo-4 and expressing RGECO-TnT were measured at 488 nm and 595 nm respectively. Emitted transients were from the same cell and therefore enabled direct pairwise comparison of T_{50} on and T_{50} off rates (n=82 cells from n=3 isolations). Data presented as mean ± SEM, * = $p<0.05$, using Wilcoxon paired t-test.

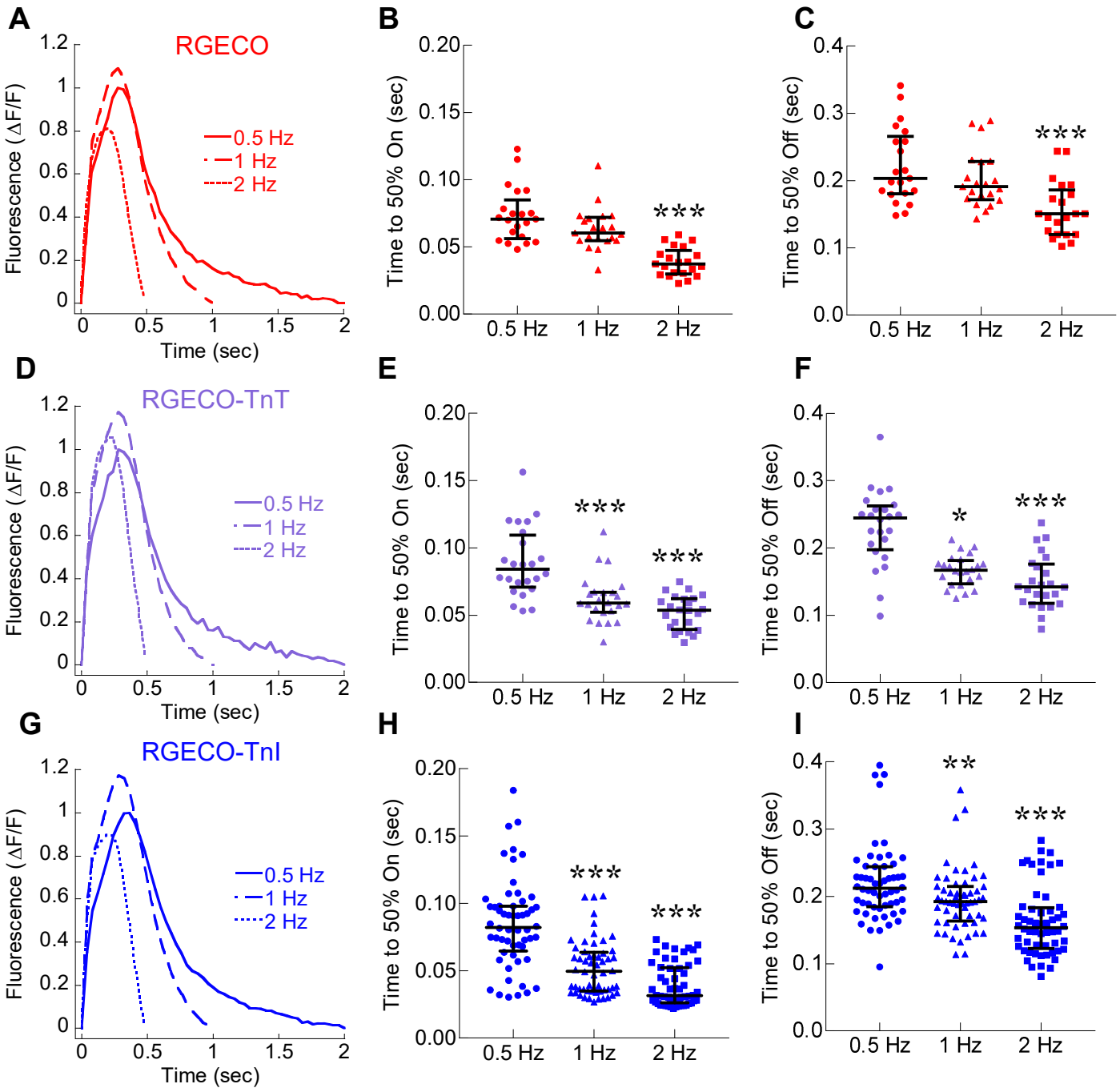

Online Figure VI. RGECO, RGECO-TnT and RGECO-TnI Ca^{2+} transients show reverse rate dependence in times to 50% on and 50% off in response to increased pacing frequency in adult GPCMs. Averaged Ca^{2+} transients of electrically paced isolated adult cardiomyocytes was used to compare pacing frequencies of 0.5 Hz, 1.0 Hz and 2 Hz using either RGECO **(A)**, RGECO-TnT **(D)** or RGECO-TnI **(G).** Adjacent dot plots show distributions of time to 50% binding, and 50% release rates across the pacing range. Shortening of both parameters is apparent for all indicators (RGECO **(B** and **C)** (n=21 cells from n=2 isolations), RGECO-TnT **(E** and **F)** (n=24 cells from n=2 isolations), and RGECO-TnI **(H** and **I)** (n=56 cells from n=3 isolations)). Lines give the median average and error bars are ± interquartile range * = p<0.05, ** = p<0.01 and *** = p<0.001 using one way ANOVA.

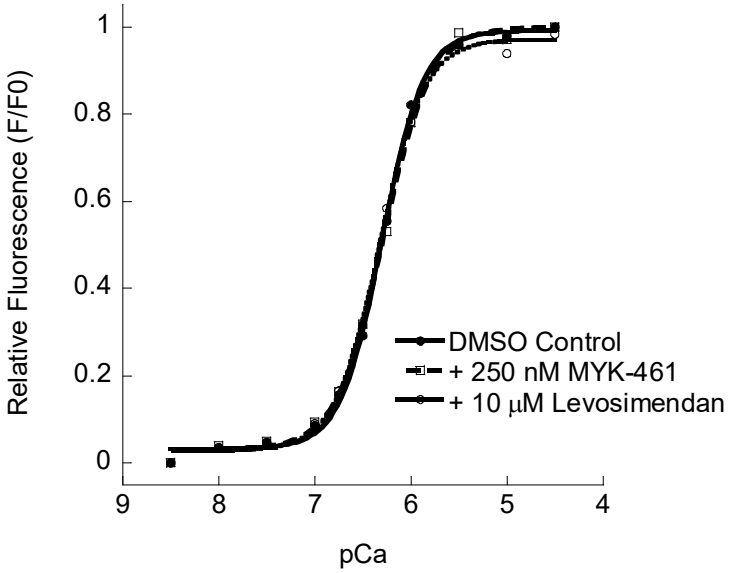

	K_d	p
Control	502 ± 23.0 nM	
MYK461	522 ± 26.9 nM	0.602
Levosimendan	475 ± 19.3 nM	0.471

Online Figure VII. MYK-461 and levosimendan had no direct effect on the function of the RGECO-TnT. Fluorescence : pCa relationship in the presence of 250 nmol/L MYK-461 and 10 μmol/L levosimendan was used to calculate the K_d values tabulated beneath (n=4). Significance values (p) were calculated using one way ANOVA.

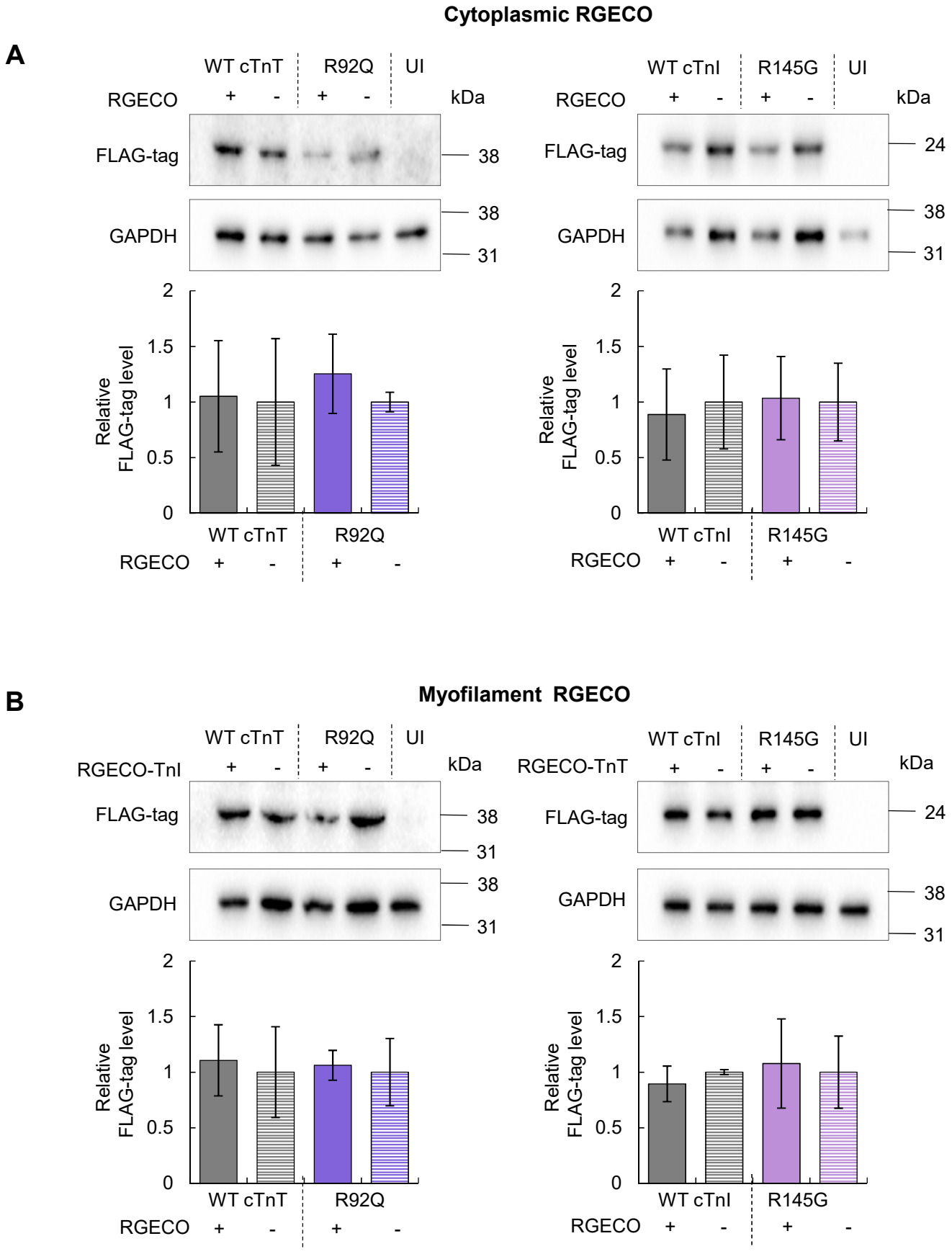

Online Figure VIII. Effect of dual transduction versus single transduction of adenoviruses on FLAG-tag expression. Western blot analysis of GPCMs transduced with WT cTnT, cTnT R92Q, WT cTnI, or cTnI R145G ± RGECO **(A)** or RGECO-TnI/RGECO-TnT **(B)**, or uninfected control (UI). Showing no significant effect on FLAG-tag expression between dual transduction with the Ca^{2+} sensor and single transduction without the Ca^{2+} sensor, n=5.

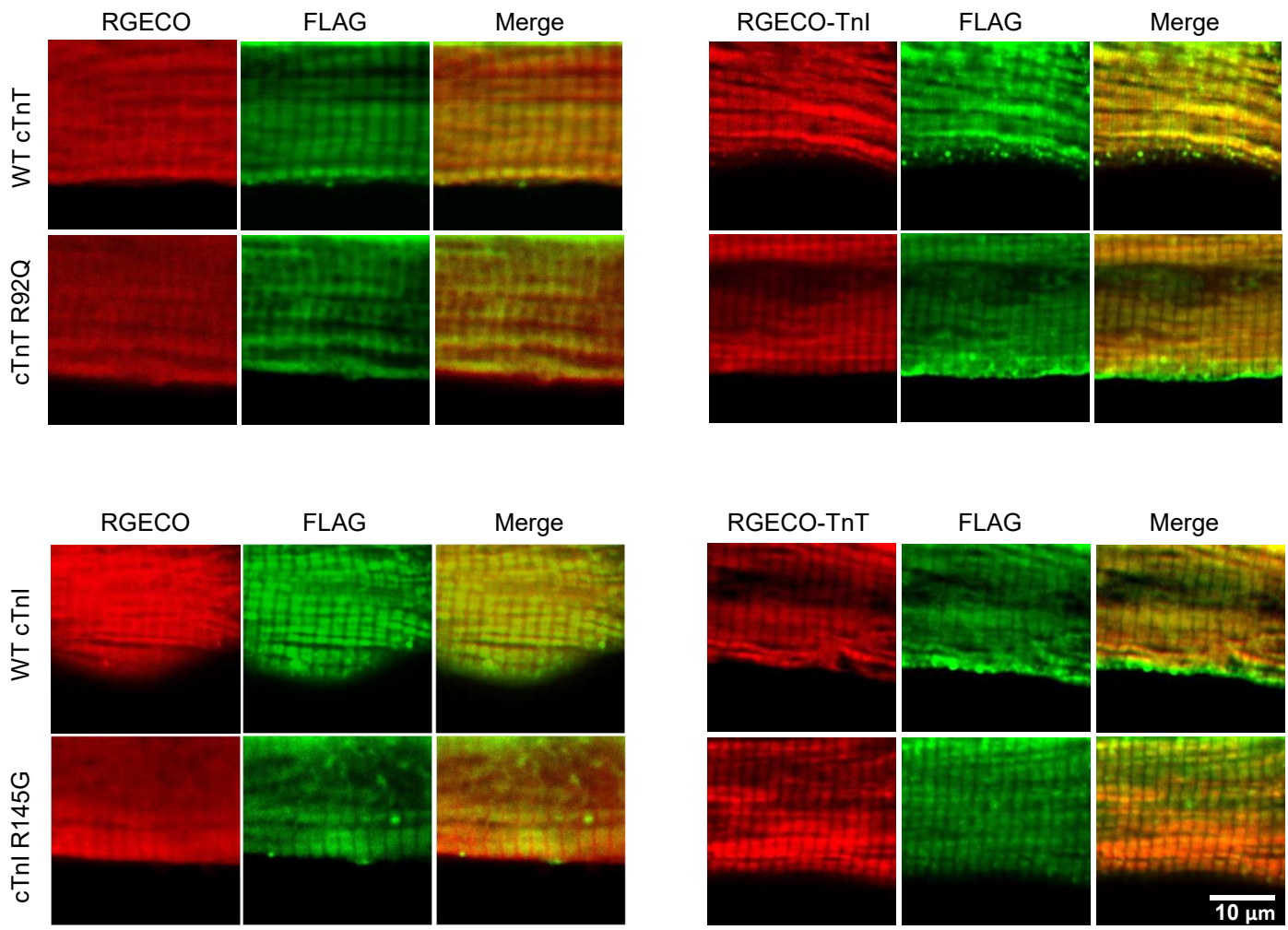

Online Figure IX. Effect of dual transduction on the localisation of FLAG-tag expressed protein. Immunofluorescence analysis of GPCMs transduced with WT cTnT, cTnT R92Q, WT cTnI, or cTnI R145G ± RGECO/RGECO-TnI/RGECO-TnT was performed using anti-FLAG tag (green) and anti-DsRed antibodies. No significant alterations to the I band localisation of FLAG-tag protein was observed between dual transduction with the Ca^{2+} sensor and previously described single transduction without the Ca^{2+} sensor.

RGECO-TnT DNA sequence

ATGGTAGACTCATCACGTCGTAAGTGGAATAAGGCAGGTCACGCAGTCAGAGCTATAGGTCGGCTGAGCTCACCCGTGGTT
TCCGAGCGGATGTACCCCGAGGACGGCGCCCTCAAGAGCGAGATCAAGAAGGGGCTGAGGCTGAAGGACGGCGGCCACTAC
GCCGCCGAGGTCAAGACCACCTACAAGGCCAAGAAGCCCGTGCAGCTGCCCGGCGCCTACATCGTAGACATCAAGTTGGAC
ATCGTGTCCCACAACGAGGACTACACCATCGTGGAACAGTGCGAACGCGCCGAGGGCCGCCACTCCACCGGCGGCATGGAC
GAGCTATACAAGGGAGGTACAGGCGGGAGTCTGGTGAGCAAGGGCGAGGAGGATAACATGGCCATCATCAAGGAGTTCATG
CGCTTCAAGGTGCACATGGAGGGCTCCGTGAACGGCCACGAGTTCGAGATCGAGGGCGAGGGCGAGGGCCGCCCCTACGAG
GCCTTTCAGACCGCTAAGCTGAAGGTGACCAAGGGTGGCCCCCTGCCCTTCGCCTGGGACATCCTGTCCCCTCAGTTCATG
TACGGCTCCAAGGCCTACATTAAGCACCCAGCCGACATCCCCGACTACTTCAAGCTGTCCTTCCCCGAGGGCTTCAGGTGG
GAGCGCGTGATGAACTTCGAGGACGGCGGCATTATTCACGTTAACCAGGACTCCTCCCTGCAGGACGGCGTATTCATCTAC
AAGGTGAAGCTGCGCGGCACCAACTTCCCCCCCGACGGCCCCGTAATGCAGAAGAAGACCATGGGCTGGGAGGCTACGCGT
GACCAACTGACTGAGGAGCAGATCGCAGAATTTAAAGAGGCTTTCTCCCTATTTGACAAGGACGGGGATGGGACGATAACA
ACCAAGGAGCTGGGGACGGTGATGCGGTCTCTGGGGCAGAACCCCACAGAAGCAGAGCTGCAGGACATGATCAATGAAGTA
GATGCCGACGGTGACGGCACATTCGACTTCCCTGAGTTCCTGACGATGATGGCAAGAAAAATGAATGACACAGACAGTGAA
GAGGAAATTAGAGAAGCGTTCCGCGTGTTTGATAAGGACGGCAATGGCTACATCGGCGCAGCAGAGCTTCGCCACGTGATG
ACAGACCTTGGAGAGAAGTTAACAGATGAGGAGGTTGATGAAATGATCAGGGTAGCAGACATCGATGGGGATGGTCAGGTA
AACTACGAAGAGTTTGTCCAAATGATGACAGCGAAGGGATCCATGTCTGACATAGAAGAGGTGGTGGAAGAGTACGAGGAG
GAGGAGCAGGAAGAAGCAGCTGTTGAAGAGCAGGAGGAGGCAGCGGAAGAGGATGCTGAAGCAGAGGCTGAGACCGAGGAG
ACCAGGGCAGAAGAAGATGAAGAAGAAGAGGAAGCAAAGGAGGCTGAAGATGGCCCAATGGAGGAGTCCAAACCAAAGCCC
AGGTCGTTCATGCCCAACTTGGTGCCTCCCAAGATCCCCGATGGAGAGAGAGTGGACTTTGATGACATCCACCGGAAGCGC
ATGGAGAAGGACCTGAATGAGTTGCAGGCGCTGATTGAGGCTCACTTTGAGAACAGGAAGAAAGAGGAGGAGGAGCTCGTT
TCTCTCAAAGACAGGATCGAGAGACGTCGGGCAGAGCGGGCCGAGCAGCAGCGCATCCGGAATGAGCGGGAGAAGGAGCGG
CAGAACCGCCTGGCTGAAGAGAGGGCTCGACGAGAGGAGGAGGAGAACAGGAGGAAGGCTGAGGATGAGGCCCGGAAGAAG
AAGGCTTTGTCCAACATGATGCATTTTGGGGGTTACATCCAGAAGCAGGCCCAGACAGAGCGGAAAAGTGGGAAGAGGCAG
ACTGAGCGGGAAAAGAAGAAGAAGATTCTGGCTGAGAGGAGGAAGGTGCTGGCCATTGACCACCTGAATGAAGATCAGCTG
AGGGAGAAGGCCAAGGAGCTGTGGCAGAGCATCTATAACTTGGAGGCAGAGAAGTTCGACCTGCAGGAGAAGTTCAAGCAG
CAGAAATATGAGATCAATGTTCTCCGAAACAGGATCAACGATAACCAGAAAGTCTCCAAGACCCGCGGGAAGGCTAAAGTC
ACCGGGCGCTGGAAATAG

RGECO-TnT amino acid sequence

MVDSSRRKWNKAGHAVRAIGRLSSPVVSERMYPEDGALKSEIKKGLRLKDGGHYAAEVKTTYKAKKPVQLPGAYIVDIKLD
IVSHNEDYTIVEQCERAEGRHSTGGMDELYKGGTGGSLVSKGEEDNMAIIKEFMRFKVHMEGSVNGHEFEIEGEGEGRPYE
AFQTAKLKVTKGGPLPFAWDILSPQFMYGSKAYIKHPADIPDYFKLSFPEGFRWERVMNFEDGGIIHVNQDSSLQDGVFIY
KVKLRGTNFPPDGPVMQKKTMGWEATRDQLTEEQIAEFKEAFSLFDKDGDGTITTKELGTVMRSLGQNPTEAELQDMINEV
DADGDGTFDFPEFLTMMARKMNDTDSEEEIREAFRVFDKDGNGYIGAAELRHVMTDLGEKLTDEEVDEMIRVADIDGDGQV
NYEEFVQMMTAKGSMSDIEEVVEEYEEEEQEEAAVEEQEEAAEEDAEAEAETEETRAEEDEEEEEAKEAEDGPMEESKPKP
RSFMPNLVPPKIPDGERVDFDDIHRKRMEKDLNELQALIEAHFENRKKEEEELVSLKDRIERRRAERAEQQRIRNEREKER
QNRLAEERARREEEENRRKAEDEARKKKALSNMMHFGGYIQKQAQTERKSGKRQTEREKKKKILAERRKVLAIDHLNEDQL
REKAKELWQSIYNLEAEKFDLQEKFKQQKYEINVLRNRINDNQKVSKTRGKAKVTGRWK.

Online Figure X. DNA and amino acid sequence of RGECO-TnT. Sequence highlighted red is RGECO, purple is human cardiac TnT and black is a BamHI cloning site which corresponds to an additional GS linker sequence in the translated amino acid.

RGECO-TnI DNA sequence

ATGGTAGACTCATCACGTCGTAAGTGGAATAAGGCAGGTCACGCAGTCAGAGCTATAGGTCGGCTGAGCTCACCCGTGGTT
TCCGAGCGGATGTACCCCGAGGACGGCGCCCTCAAGAGCGAGATCAAGAAGGGGCTGAGGCTGAAGGACGGCGGCCACTAC
GCCGCCGAGGTCAAGACCACCTACAAGGCCAAGAAGCCCGTGCAGCTGCCCGGCGCCTACATCGTAGACATCAAGTTGGAC
ATCGTGTCCCACAACGAGGACTACACCATCGTGGAACAGTGCGAACGCGCCGAGGGCCGCCACTCCACCGGCGGCATGGAC
GAGCTATACAAGGGAGGTACAGGCGGGAGTCTGGTGAGCAAGGGCGAGGAGGATAACATGGCCATCATCAAGGAGTTCATG
CGCTTCAAGGTGCACATGGAGGGCTCCGTGAACGGCCACGAGTTCGAGATCGAGGGCGAGGGCGAGGGCCGCCCCTACGAG
GCCTTTCAGACCGCTAAGCTGAAGGTGACCAAGGGTGGCCCCCTGCCCTTCGCCTGGGACATCCTGTCCCCTCAGTTCATG
TACGGCTCCAAGGCCTACATTAAGCACCCAGCCGACATCCCCGACTACTTCAAGCTGTCCTTCCCCGAGGGCTTCAGGTGG
GAGCGCGTGATGAACTTCGAGGACGGCGGCATTATTCACGTTAACCAGGACTCCTCCCTGCAGGACGGCGTATTCATCTAC
AAGGTGAAGCTGCGCGGCACCAACTTCCCCCCCGACGGCCCCGTAATGCAGAAGAAGACCATGGGCTGGGAGGCTACGCGT
GACCAACTGACTGAGGAGCAGATCGCAGAATTTAAAGAGGCTTTCTCCCTATTTGACAAGGACGGGGATGGGACGATAACA
ACCAAGGAGCTGGGGACGGTGATGCGGTCTCTGGGGCAGAACCCCACAGAAGCAGAGCTGCAGGACATGATCAATGAAGTA
GATGCCGACGGTGACGGCACATTCGACTTCCCTGAGTTCCTGACGATGATGGCAAGAAAAATGAATGACACAGACAGTGAA
GAGGAAATTAGAGAAGCGTTCCGCGTGTTTGATAAGGACGGCAATGGCTACATCGGCGCAGCAGAGCTTCGCCACGTGATG
ACAGACCTTGGAGAGAAGTTAACAGATGAGGAGGTTGATGAAATGATCAGGGTAGCAGACATCGATGGGGATGGTCAGGTA
AACTACGAAGAGTTTGTCCAAATGATGACAGCGAAGCTCGAGATGGCGGATGGGAGCAGCGATGCGGCTAGGGAACCTCGC
CCTGCACCAGCCCCAATCAGACGCCGCTCCTCCAACTACCGCGCTTATGCCACGGAGCCGCACGCCAAGAAAAAATCTAAG
ATCTCCGCTTCTAGAAAATTGCAGCTGAAGACTCTGCTGCTGCAGATTGCAAAGCAAGAGCTGGAGCGAGAGGCGGAGGAG
CGGCGCGGAGAGAAGGGGCGCGCTCTGAGCACCCGCTGCCAGCCGCTGGAGTTGACCGGGCTGGGCTTCGCGGAGCTGCAG
GACTTGTGCCGACAGCTCCACGCCCGTGTGGACAAGGTGGATGAAGAGAGATACGACATAGAGGCAAAAGTCACCAAGAAC
ATCACGGAGATTGCAGATCTGACTCAGAAGATCTTTGACCTTCGAGGCAAGTTTAAGCGGCCCACCCTGCGGAGAGTGAGG
ATCTCTGCAGATGCCATGATGCAGGCGCTGCTGGGGGCCCGGGCTAAGGAGTCCCTGGACCTGCGGGCCCACCTCAAGCAG
GTGAAGAAGGAGGACACCGAGAAGGAAAACCGGGAGGTGGGAGACTGGCGGAAGAACATCGATGCACTGAGTGGAATGGAG
GGCCGCAAGAAAAAGTTTGAGAGCTGA

RGECO-TnI amino acid sequence

MVDSSRRKWNKAGHAVRAIGRLSSPVVSERMYPEDGALKSEIKKGLRLKDGGHYAAEVKTTYKAKKPVQLPGAYIVDIKLD
IVSHNEDYTIVEQCERAEGRHSTGGMDELYKGGTGGSLVSKGEEDNMAIIKEFMRFKVHMEGSVNGHEFEIEGEGEGRPYE
AFQTAKLKVTKGGPLPFAWDILSPQFMYGSKAYIKHPADIPDYFKLSFPEGFRWERVMNFEDGGIIHVNQDSSLQDGVFIY
KVKLRGTNFPPDGPVMQKKTMGWEATRDQLTEEQIAEFKEAFSLFDKDGDGTITTKELGTVMRSLGQNPTEAELQDMINEV
DADGDGTFDFPEFLTMMARKMNDTDSEEEIREAFRVFDKDGNGYIGAAELRHVMTDLGEKLTDEEVDEMIRVADIDGDGQV
NYEEFVQMMTAKLEMADGSSDAAREPRPAPAPIRRRSSNYRAYATEPHAKKKSKISASRKLQLKTLLLQIAKQELEREAEE
RRGEKGRALSTRCQPLELTGLGFAELQDLCRQLHARVDKVDEERYDIEAKVTKNITEIADLTQKIFDLRGKFKRPTLRRVR
ISADAMMQALLGARAKESLDLRAHLKQVKKEDTEKENREVGDWRKNIDALSGMEGRKKKFES.

Online Figure XI. DNA and amino acid sequence of RGECO-TnI. Sequence highlighted red is RGECO, blue is human cardiac TnI and black is a XhoI cloning site which corresponds to an additional LE linker sequence in the translated amino acid.

	GFP-TnT	TnT-GFP	GFP-TnI	TnI-GFP	GFP-TnC	TnC-GFP
ΔpCa_{50}	-0.031±0.018	-0.149±0.056	0.028±0.015	-0.279±0.624	0.564±0.269	-0.369±0.125
Δn_H	0.980±0.691	7.308±3.703	0.505±1.085	**-2.158±0.170 ****	0.8649±0.598	-0.867±0.912
ΔMin (sec^{-1})	0.548±0.219	0.185±0.089	0.235±0.114	**3.096±1.105 ***	**6.551±0.969 *****	**5.382±1.874 ***
ΔMax (sec^{-1})	0.686±0.588	**-2.958±0.399 ***	-0.036±0.270	0.787±0.457	1.479±0.798	**1.439±0.545 ***

Online Table I. Extracted parameters from *in vitro* actin activated acto-myosin S1 ATPase assays performed to investigate myofilament function in the presence of GFP conjugates of the troponin complex. Δ values from paired experimental comparisons for pCa_{50}, n_H, maximum and minimum activity (sec^{-1}) with standard error and significance. n=5, significance values comparing unconjugated with GFP conjugated troponin are $p<0.001$=***, $p<0.01$=** and $p<0.05$=* using a students t-test.

	RGECO	RGECO-TnT	RGECO-TnI
K_d at 25 °C (nM)	1607	1186	1105
K_d at 37 °C (nM)	860	764	657
Quantum Yield pCa 4.5 (Φ)	0.20	0.33	0.3
Quantum Yield pCa 8.5 (Φ)	0.06	0.11	0.1
Molar Extinction coefficent pCa 4.5 (ε (mM^{-1}•cm^{-1})) (565 nm)	32.39	34.53	35.87
Molar Extinction coefficent pCa 8.5 (ε (mM^{-1}•cm^{-1})) (565 nm)	5.17	6.64	6.85
Molar Extinction coefficent pCa 4.5 (ε (mM^{-1}•cm^{-1})) (455 nm)	4.16	6.18	6.2
Molar Extinction coefficent pCa 8.5 (ε (mM^{-1}•cm^{-1})) (455 nm)	11.25	14.11	16.36
Brightness pCa 4.5 (mM^{-1}•cm^{-1})	6.48	11.30	13.58
Brightness pCa 8.5 (mM^{-1}•cm^{-1})	0.31	0.73	1.21
Intensity change ± Ca^{2+}	10.18x	10.33x	11.25x

Online Table II. Extracted parameters from fluorescence and absorbance spectra and kinetic experiments.
Brightness is defined as the product of ε and Φ.

Sensor	*n*	Time to 50% Ca^{2+} Binding (sec)	Time to 50% Ca^{2+} Release (sec)
RGECO	*108*	0.058±0.003	0.308±0.012
RGECO-TnT	*55*	**0.105±0.007** ***	**0.282±0.011** **
RGECO-TnI	*112*	**0.097±0.004** ***	**0.267±0.006** ***

Online Table III. Extracted parameters of GPCM Ca^{2+} transients transduced with RGECO, RGECO-TnT or RGECO-TnI. Extracted values from a paired comparison of GPCMs adenovirally transduced with RGECO, RGECO-TnT or RGECO-TnI. *n* = total cell number from at least 3 separate cell isolations, ± = standard error. Significance values comparing RGECO to RGECO-TnT or RGECO-TnI are $p<0.01$ = ** and $p<0.001$ = ***. RGECO-TnT verses RGECO-TnI = ns for all parameters, using a Kruskal Wallis non parametric test.

A

Sensor	Mutant	*n*	Relative RGECO Peak Intensity	Time to 50% Ca^{2+} Binding (sec)	Time to 50% Ca^{2+} Release (sec)	Time of Peak (sec)
RGECO	WT cTnT	*94*	1.00±0.041	0.066±0.002	0.219±0.006	0.288±0.007
RGECO	cTnT R92Q	*94*	0.99±0.045	**0.102±0.004** ***	**0.247±0.006** **	**0.365±0.007** ***
RGECO	WT cTnI	*107*	1.00±0.037	0.070±0.002	0.198±0.004	0.281±0.006
RGECO	cTnI R145G	*103*	**1.60±0.058** ***	**0.083±0.002** ***	**0.255±0.005** ***	**0.345±0.008** ***

B

Sensor	Mutant	*n*	Relative RGECO Peak Intensity	Time to 50% Ca^{2+} Binding (sec)	Time to 50% Ca^{2+} Release (sec)	Time of Peak (sec)
RGECO-TnI	WT cTnT	*102*	1.00±0.039	0.087±0.003	0.194±0.004	0.333±0.007
RGECO-TnI	cTnT R92Q	*115*	**1.32±0.053** ***	**0.128±0.005** ***	**0.247±0.004** ***	**0.424±0.008** ***
RGECO-TnT	WT cTnI	*123*	1.00±0.030	0.082±0.003	0.202±0.005	0.338±0.008
RGECO-TnT	cTnI R145G	*127*	**1.16±0.042** **	**0.094±0.003** **	**0.247±0.005** ***	**0.391±0.010** ***

Online Table IV. Extracted parameters of GPCMs transduced with RGECO or myofilament localised RGECO and WT/HCM mutant troponin. Extracted Ca^{2+} transient values from GPCMs adenovirally transduced with RGECO (**A**) or RGECO-TnI/RGECO-TnT (**B**) and either WT cTnT, cTnT R92Q, WT cTnI, or cTnI R145G. *n* = total cell number from at least 3 separate cell isolations, ± = standard error. Significant values comparing either WT cTnT to cTnT R92Q or WT cTnI to cTnI R145G are $p<0.001$ = ***, or $p<0.01$ = ** using a Mann Whitney test.